Chapter-5

Tribological evaluation of biolubricants with ZDDP additive, various oxides and polymeric nano-additives

This chapter covers the tribological evaluation of the additive based biolubricants using four-ball tester. Different nanoparticles (oxides and polymeric) have been used in biolubricants to formulate the nanolubricants. The tribo-performance of the vegetable based nanolubricants was compared with the paraffin oil (as base lubricant) and zinc dialkyldithiophosphate (ZDDP) as an additive at similar compositions. Paraffin oil and ZDDP are used in various applications but both are hazardous to the environment during its life span.

5.1. Morphology and size of the nanoparticles

5.1.1. Calcium-copper-titanate (CCTO) nanoparticles

5.1.1.1. Phase analysis of synthesized CCTO nanoparticles

X-ray diffraction (XRD) image of synthesized CCTO nanoparticles is shown in Figure 5.1.The obtained peaks of maximum intensity to the minimum intensity at 2θ angles (Cu K-α radiation and 2θ angle ranging from 10° to 80°) presented in Table 5.1. All the X-ray diffraction peaks match well with the standard powder diffraction pattern (JCPDS Card number: 75-2188), it confirms the successful synthesis of single phase CCTO nanoparticles.

The crystallite size calculation has been done using Debye-Scherrer Eq.5.1:

$$t = \frac{0.9\,\lambda}{B\cos\theta} \qquad (5.1)$$

Where t: crystallite size, λ: X-ray Cu K-α wavelength (≈ 0. 15406 nm), B: full width at half maxima, θ: half of diffraction angle 2θ. The mean crystallite size calculated by using Eq.5.1 and it was 45.6 nm approximately.

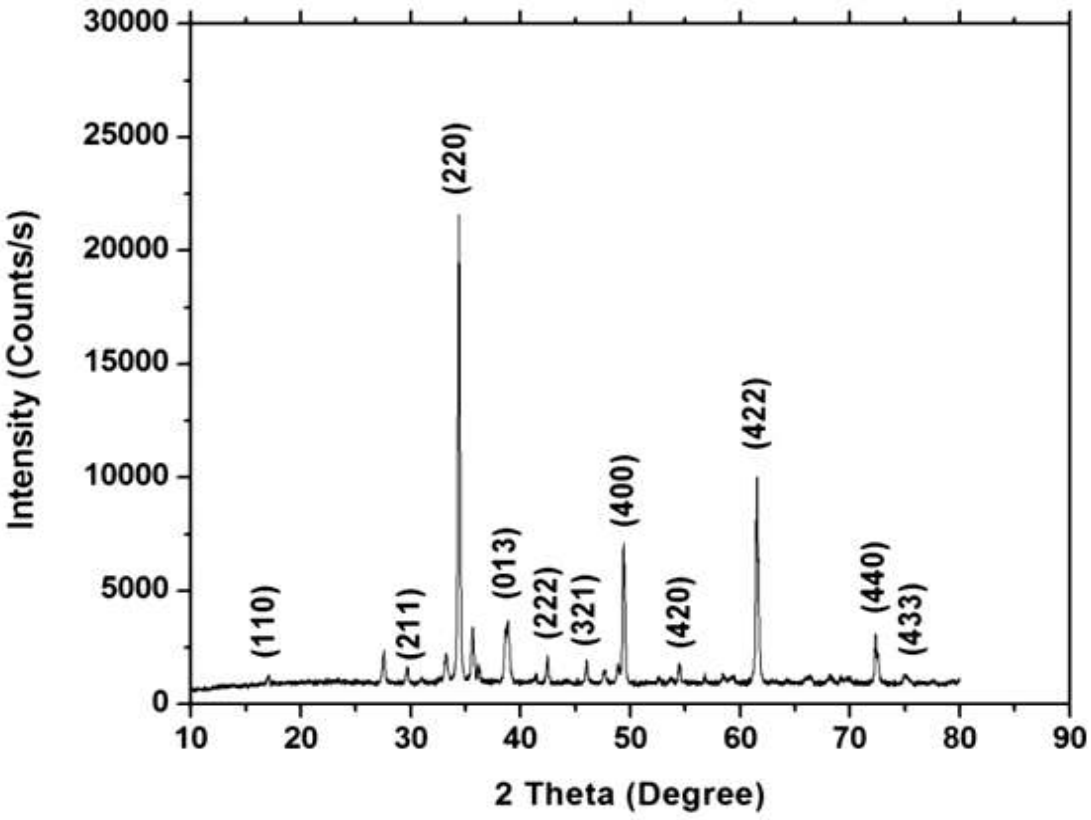

Figure 5.1. XRD pattern of CCTO nanoparticles calcined at 800°C for 6 hours.

Table 5.1: Diffraction angle and corresponding Miller plane (h k l) from maximum to minimum intensity of XRD pattern.

Diffraction angle (2θ)	Corresponding (h k l) plane
34.42°	(2 2 0)
61.5°	(4 2 2)
49.4°	(4 0 0)
38.68°	(0 1 3)
72.56°	(4 4 0)
42.48°	(2 2 2)
45.90°	(3 2 1)
29.58°	(2 1 1)
16.95°	(1 1 0)
74.85°	(4 3 3)

5.1.1.2. Elemental analysis of synthesized CCTO nanoparticles

The Energy dispersive spectroscopy (EDS) of the synthesized nanoparticles has been depicted in Figure 5.2. The obtained peaks reveal the presence of Ca, Ti, Cu, C, O elements confirming the formation of CCTO phase. The CCTO is a ceramic and non-conductive particle therefore a very thin gold coating was done to make them conductive for performing EDS analysis.

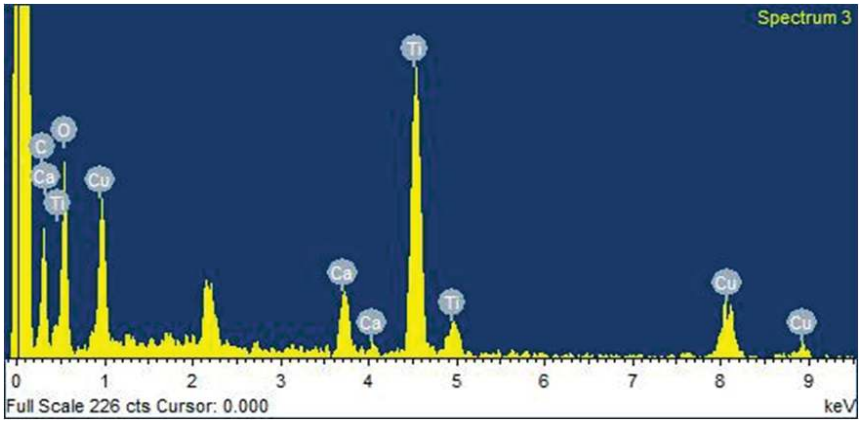

Figure 5.2. EDS of synthesized CCTO nanoparticles.

5.1.1.3. Particle size and morphology

Figure 5.3 represents the topography of the synthesized CCTO nanoparticles. The size of the synthesized nanoparticles was analyzed using TEM, and it was measured by Image J software.

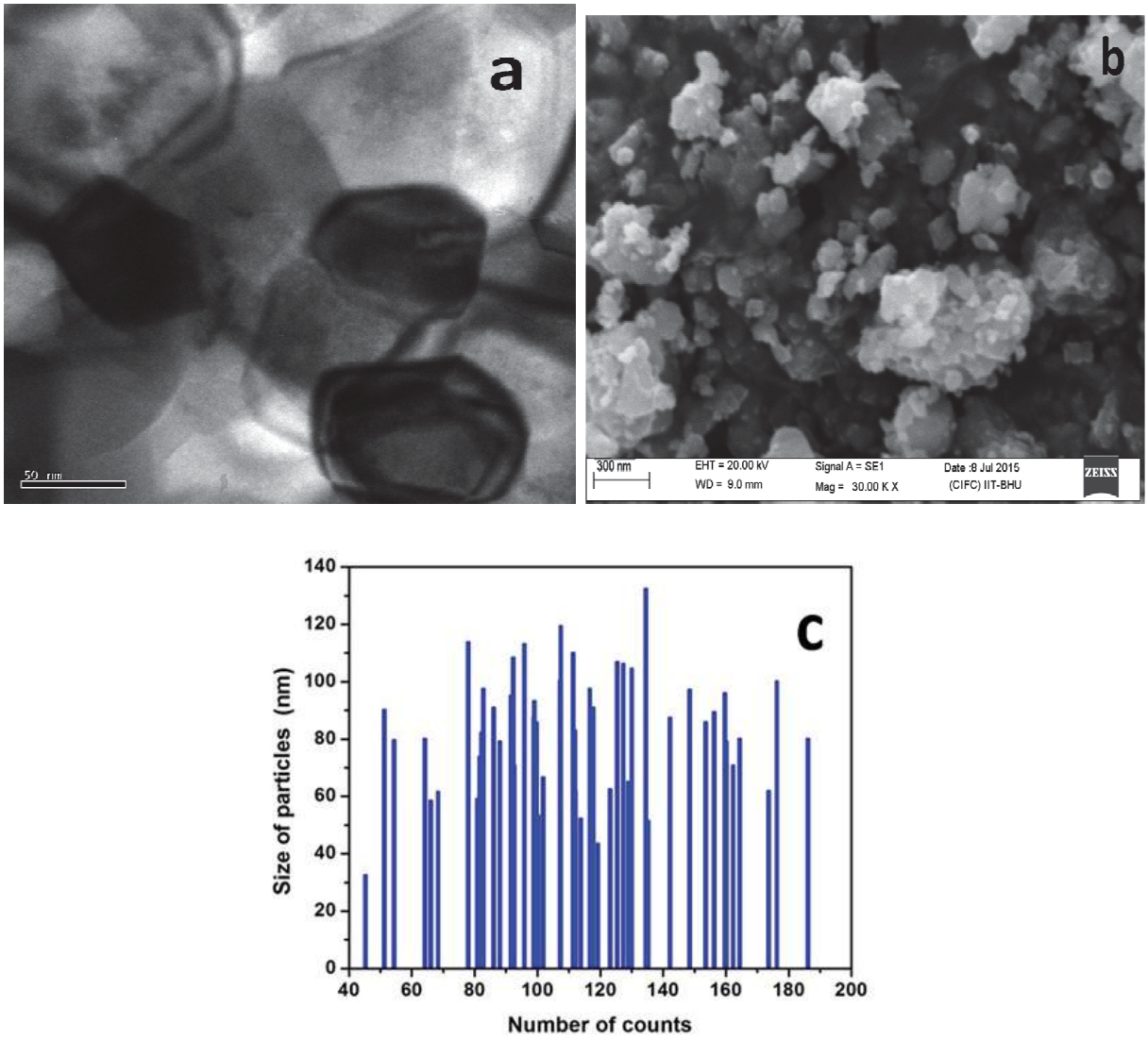

Figure 5.3. Images representing (a) TEM, (b) SEM and (c) nanoparticles size variation for synthesized CCTO nanoparticles.

TEM image of CCTO nanoparticles is presented in Figure 5.3a. The measurements of 50 CCTO nanoparticles were carried out, and the average calculated size was approximately 83 nm. All the particles were approximately spherical. The crystallite size calculated by using Debye Scherrer formula (Eq.5.1) was smaller than the TEM particle size measurement this is because Scherrer formula neither considers the lattice strain effect nor instrumental factor on the peak broadening. Figure 5.3b represents the SEM image of synthesized CCTO particles which shows approximately spherical and regular morphology. The minute agglomeration of nanoparticles was observed; however, the particles were uniformly dispersed in the base oil with proper ultrasonication. The size variations of nanoparticles are depicted in the Figure 5.3c. The particle size varies from 33 -132 nm, however, most of the particles were within the range from 60 to 90 nm, and this confirms the average size of the nanoparticles, which was obtained through TEM and SEM.

5.1.2. CeO_2 nanoparticles

Figure 5.4 depicts the size and morphology of the CeO_2 nanoparticles. It was observed that the shape of CeO_2 nanoparticles was almost spherical and the average size was approximately 80 nm. The CeO_2 nanoparticle size varied from 34.2 to 121 nm, with most in the range of 65 to 90 nm.

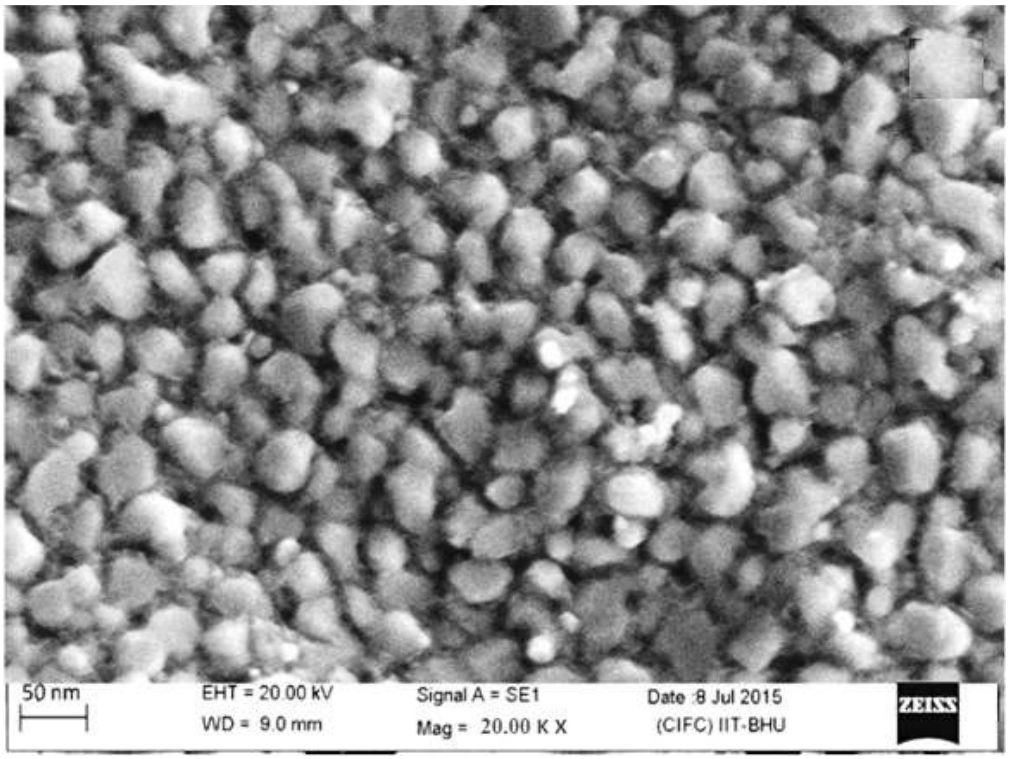

Figure 5.4. SEM image of CeO_2 nanoparticles.

5.1.3. CuO and surface modified CuO nanoparticles

The surface of the CuO nanoparticle was modified with sodium dodecyle sulfate (SDS) to produce surface treated CuO nanoparticles and abbreviated as S-CuO.

5.1.3.1. Surface treatment

The capping of the nanoparticles is one of the economical and effective surface treatment processes. The capping of surfactant helps in the reduction of van der Walls attraction force among the particles by dominating the electric double layer repulsive force. It results in achieving the stable suspension of nanoparticles in the base oils. Therefore, SDS has been capped over the nanoparticle's surface by the chemical method to make the proper suspension. Three-neck round flask, magnetic stirrer, and condensation system have been

used in the capping process. The weight ratio (CuO: SDS) of 1:5 used for modification. Initially, a calculated amount of SDS was dissolved in the ethanol, heated and stirred at 70°C via the magnetic stirrer-cum-hot plate. After that, the calculated amount of CuO nanoparticles were added to a dissolved SDS solution and stirred continuously for 24 hours. After the completion of the reaction, nanoparticles were separated with filter paper and washed with hot ethanol and dried. The dried nanoparticles were crushed with pestle and mortar to obtain the final product.

5.1.3.2. Confirmation of S-CuO formation

FTIR was used to ensure the capping of SDS over the nanoparticles surface. FTIR analysis of modified and unmodified nanoparticles was carried out by preparing the pellets. These thin pellet samples were composed of 99% potassium bromide (KBr) and 1% of nanoparticles sample. The nanoparticles and KBr were thoroughly mixed with pestle and mortar and put into the three piece-die-set. The mixture pressed in hand-press assembly for few minutes. Under high pressure, the KBr start to flow, and by releasing the pressure a transparent sheet (pellet) was formed. This pellet neither reacts with the sample nor shows an absorption spectrum in the infrared region.

The characteristic spectra of unmodified CuO nanoparticles, SDS and modified S-CuO nanoparticles have been presented in Figure 5.5. The characteristic bands of SDS molecules can be divided into two regions, i.e. aliphatic and sulfonic acid. Aliphatic acid represents tail group while sulfonic acid as head group. The two characteristic peaks at wavenumber 2767 and 2889 cm^{-1} represent symmetric and asymmetric stretching vibration of the aliphatic tail

group. However, a peak at 1196 cm^{-1} represents a head group of SDS molecules (Soomro et al. 2014).

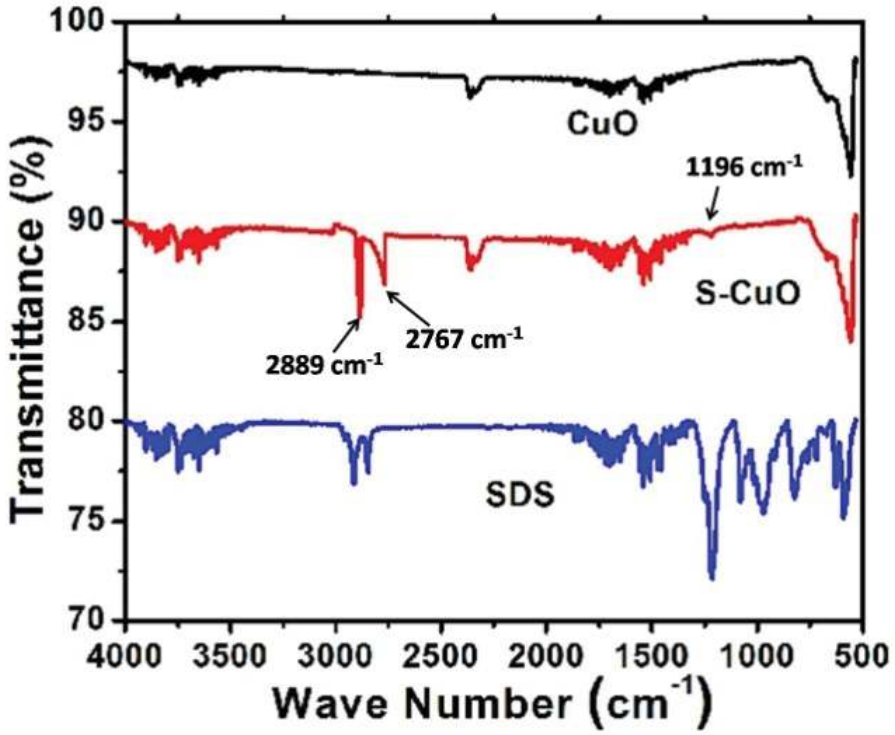

Figure 5.5. FTIR spectra of SDS, CuO and S-CuO.

Moreover, the band of SDS at 1192 cm^{-1} was red-shifted to 1196 cm^{-1} for surface treated nanoparticles. It indicates that capping of SDS on the CuO nanoparticle is due to negatively charged head group moiety (Soomro et al. 2014; Hosseinpour et al. 2012). Also, these characteristic peaks (i.e., at 2889 and 2767 cm^{-1}) are absent in the unmodified CuO spectrum, while it was present in the SDS spectrum. From the perceived spectrum, it can be inferred that CuO nanoparticles had been successfully modified by using SDS and formed S-CuO.

5.1.3.3. Size and morphology of S-CuO

Figure 5.6 depicts the SEM image of CuO and surface capped S-CuO nanoparticles. Image J software was used to measure the dimensions of 100 nanoparticles.

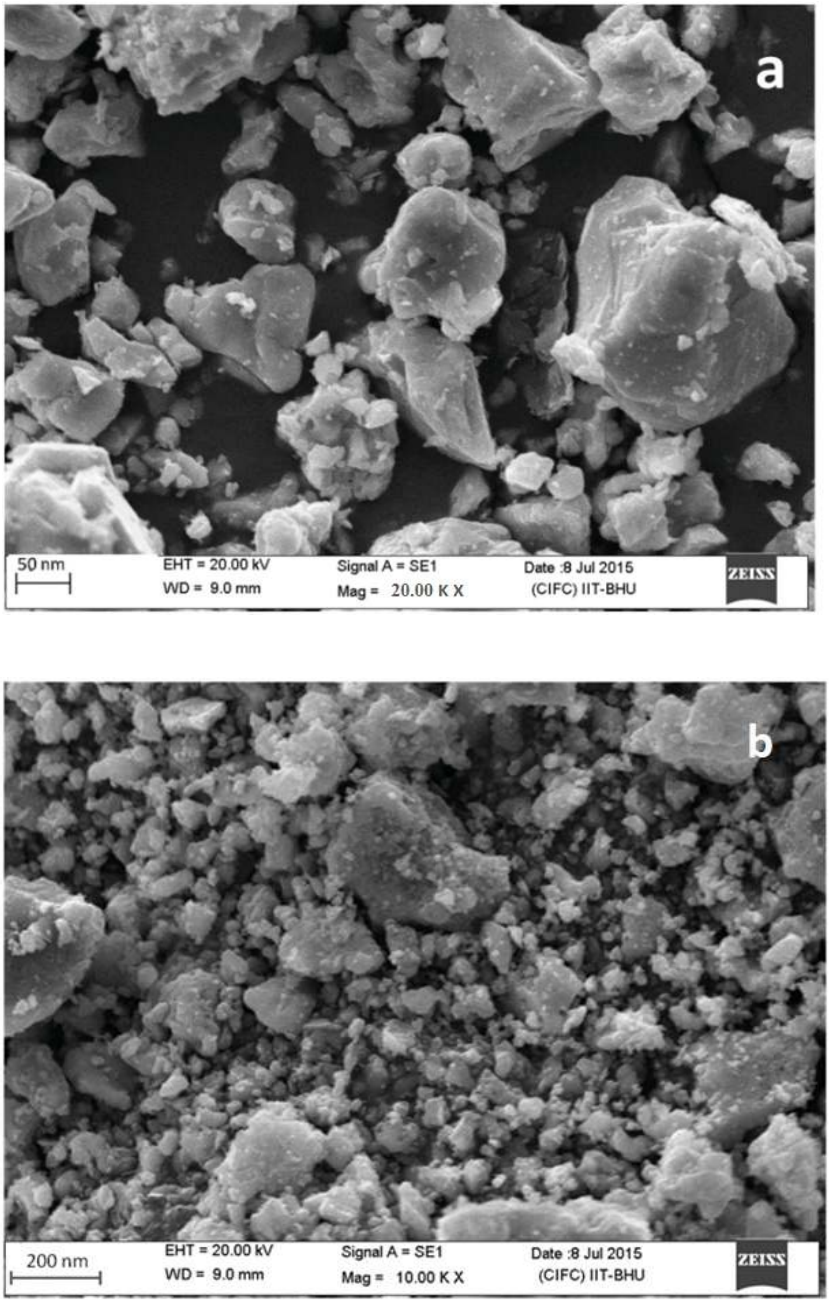

Figure 5.6. The SEM topography of (a) CuO and (b) S-CuO nanoparticles.

The average size of unmodified and modified nanoparticles after the modification was observed to be approximately 80 nm (variation between 32.7 to 124.1 nm) and 151.2 nm

respectively. While the manufacturer specification mentioned was less than 50 nm. It might be due to coalescence of the nanoparticles due to cohesive force between the particles as well as capping with SDS. The nanoparticles were a combination of spherical and regular in shape; however, few of the nanoparticles were irregular.

5.1.4. PTFE nanoparticles

The morphology of PTFE nanoparticles depicted in Figure 5.7. It was observed that the PTFE nanoparticles are spherical in shape. The average size of 50 particles was approximately 90.4 nm. The PTFE nanoparticle size varied from 43 to 107.8 nm.

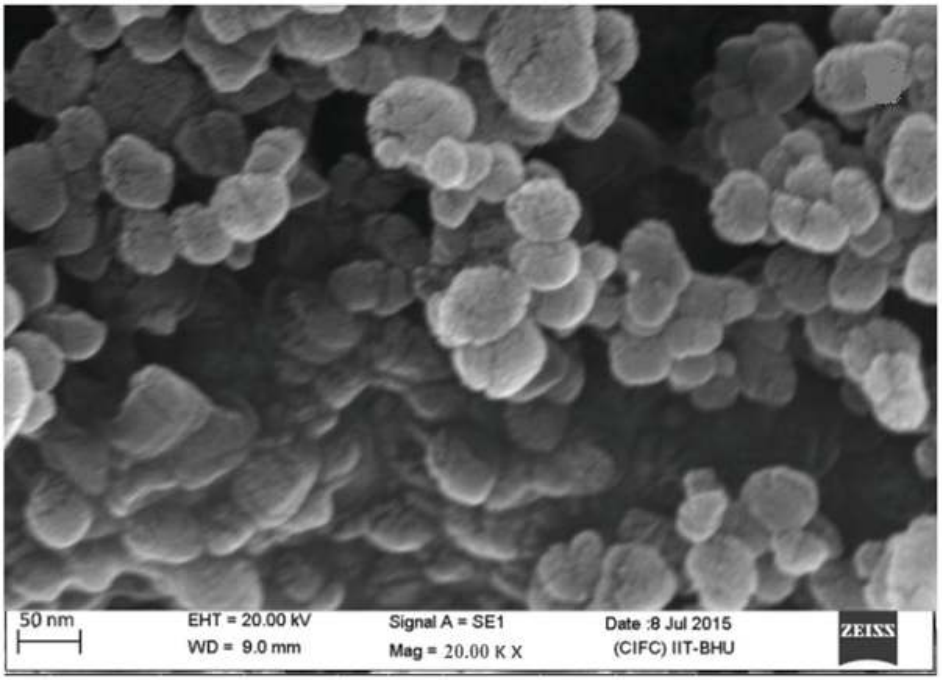

Figure 5.7. SEM image of PTFE nanoparticles.

5.2. Formulation of nanolubricants and suspension stability of nanoparticles

The nanolubricant formulated with the addition of the nanoparticles (also called nano-additive) in raw oil. The measured amount of nano-additives was blended in the oil

vigorously using magnetic stirrer for one hour without heating. After the uniform mixing of nano-additives in the raw oil, the blended solution is kept in the ultrasonicator for one hour. It enhanced the suspension stability of the nano-additive. About 0.1 wt% of SDS (as a dispersant) was used in the nanolubricants. In case of the CuO, the surface of nanoparticles was treated in place of direct addition. The nanolubricant for testing was obtained after the ultrasonication. The typical suspension images of S-CuO based lubricant is depicted in Figure 5.8.

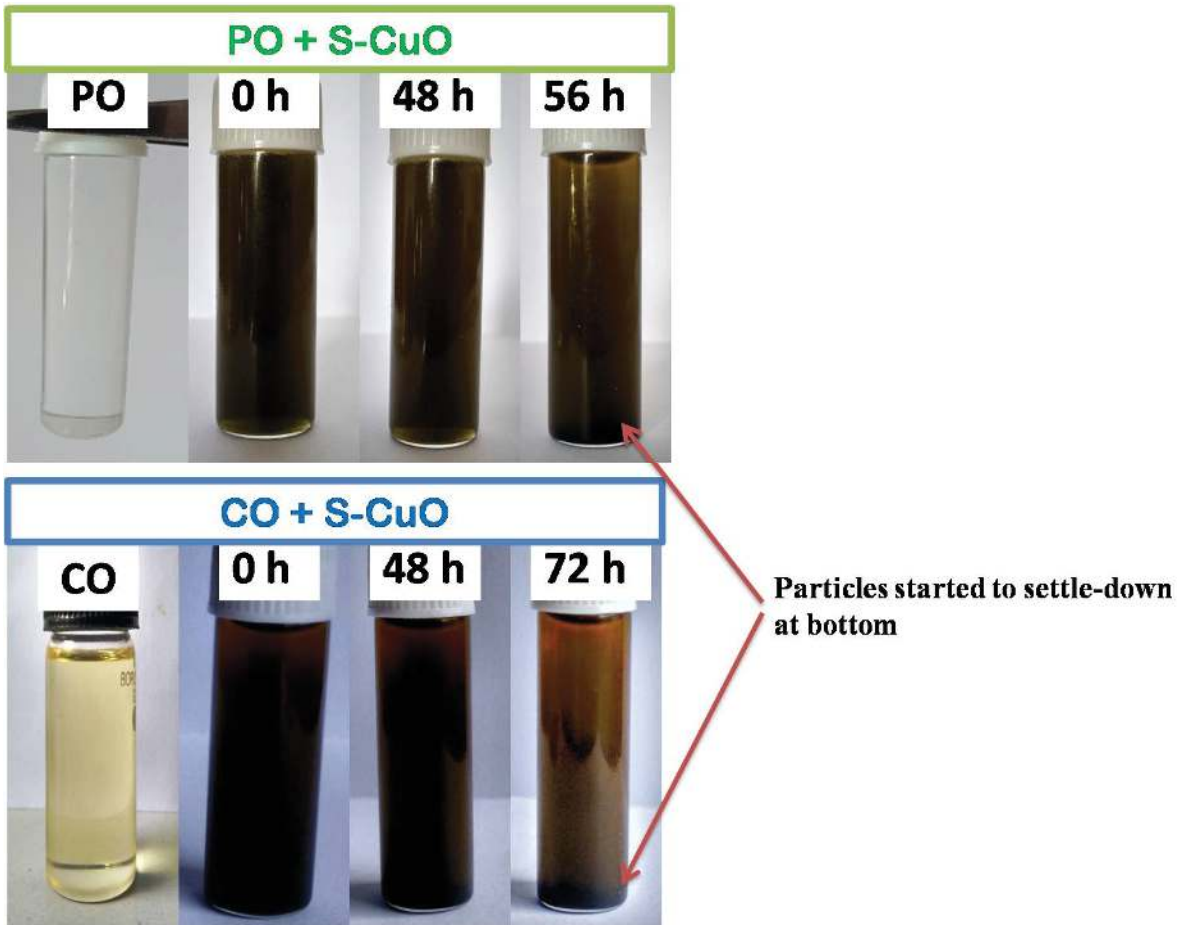

Figure 5.8. Typical suspension stability images S-CuO based nanolubricant.

In Figure 5.8 the 0h represents the formulated nanolubricant just after the ultrasonication. And, rest of the notations (like 48h, 56h, 72h, etc.) are represented according to the elapsed time (in hours) and it is up to the final settle down of the nanoparticles at the bottom of the jar for various lubricants. Initially at 0h, the nanolubricant showing uniform nanoparticle distribution in all types of the oil tested and it was in full black in colour. However, with elapsed time the particles tend to agglomerate, which changes the solution colour.

5.3. Tribological results and discussion

The antiwear, antifriction and EP behavior of the different biolubricants evaluated with different types of the additives (ZDDP and nano-additives). And, the tribo-performance of the additive based biolubricant compared with the paraffin oil with the similar level of concentrations. In this study, 0.1 and 0.25%w/v concentrations were considered as lower concentration range, while 0.5 and 1.0%w/v as higher concentration range. The tribological results have been presented additive-wise in further sections of the discussion.

5.3.1. Evaluation of tribo-performance for ZDDP and CCTO based lubricants

5.3.1.1. Antiwear study

The wear scar variations presented in Figure 5.9 and 5.10 for different compositions of castor oil (CO) and paraffin oil (PO), respectively. The magnitude of wear scar diameter (WSD) presented in Table 5.2. Here CZ, PZ, CC, and PC referred to the CO + ZDDP, PO + ZDDP, CO + CCTO, and PO + CCTO, respectively. And, 0.1, 0.25, 0.5, 1.0 prefix are referred to the %w/v concentration in base oils. The concentration of additives was limited to 1.0 w/v% because it may saturate in the base oil. However, the saturation concentration depends upon intrinsic property of raw oil and the nanoparticles.

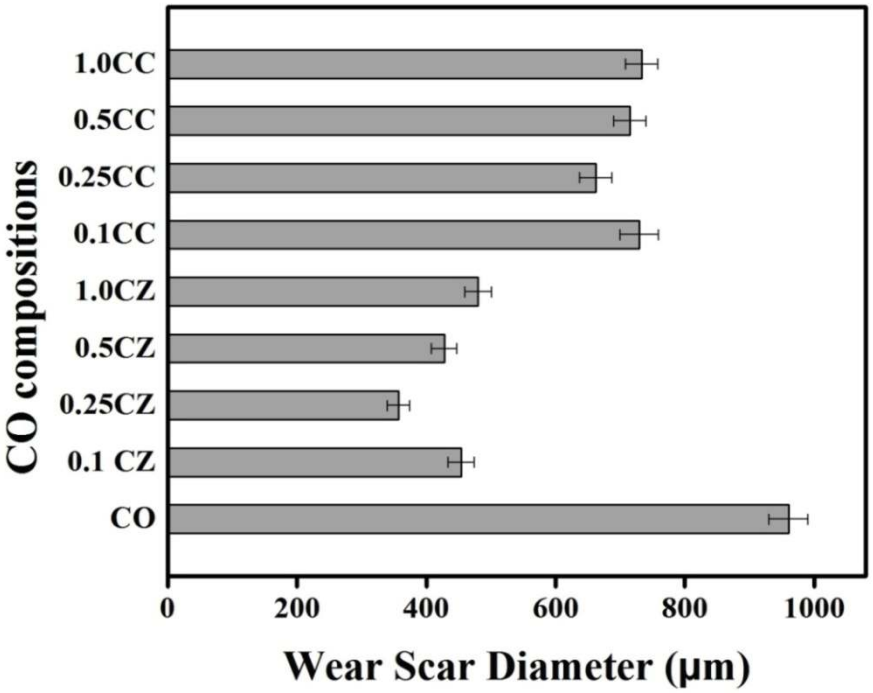

Figure 5.9. Variations in WSD for different castor oil compositions with CCTO and ZDDP tested at 392N load for 1h.

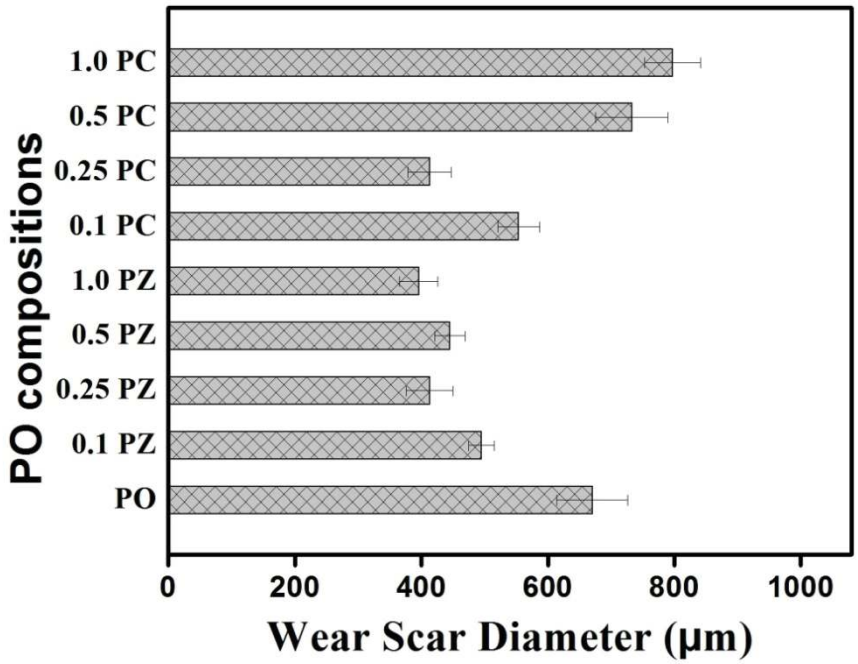

Figure 5.10. Variations in WSD for different paraffin oil compositions with CCTO and ZDDP tested at 392N load for 1h.

Table 5.2. WSD for different concentration of ZDDP and CCTO in CO and PO.

Oil composition	WSD (µm)	Oil composition	WSD (µm)
CO	906.4	***PO***	670.3
0.1CZ	454.2	***0.1PZ***	495.1
0.25CZ	357.4	***0.25PZ***	414.2
0.5CZ	427.8	***0.5PZ***	445.3
1.0CZ	480.5	***1.0PZ***	395.6
0.1CC	729.5	***0.1PC***	553.7
0.25CC	662.1	***0.25PC***	413.1
0.5CC	715.0	***0.5PC***	732.4
1.0CC	733.0	***1.0PC***	796.9

In case of castor oil compositions, the highest WSD was observed for the CO, i.e. 906.4 µm, whilst for CO with additives reduced the WSD significantly. ZDDP concentrations of 0.1, 0.25, 0.5 and 1.0 %w/v have shown WSD as 454.2, 357.4, 427.8 and 480.5 µm, respectively, whereas similar concentration level of CCTO nanoparticles has shown WSD as 729.5, 662.17, 715 and 733 µm, respectively. The variation in WSD for CO with ZDDP and CCTO admixture was 2.4 and 3.1%, respectively (Figure 5.9). Zhiwei et al. (2014) and Luo et al. (2014) also reported analogous variation in wear scar size by variation in nanoparticles concentrations in the base oil. For both ZDDP and CCTO, 0.25 w/v% amount was optimum because of the minimum WSD. At an optimum concentration of ZDDP and CCTO the maximum reductions in the WSD were 62.7 and 31.05 %, respectively, in comparison to CO.

Figure 5.11 and 5.12 shows the images of SEM and AFM surface roughness of the worn surfaces at the optimum concentration. One could observe a heavily grooved (3-D view) worn surface in Figure 5.12 representing a close surface contact and indicate that the system was working under boundary lubrication regime. A typical power spectral density (PSD) spectrum for the worn surface lubricated with castor oil with 0.25%w/v CCTO presented in Figure 5.12g. It shows that the most of the major grooves (in Figure 5.12 e and f) varied from 74 to 88 nm. Thus, a heavy groove has been formed by CCTO particles whose sizes were in the range between 70-90 nm. By calculation with Eq 3.5 and 3.6 (in Chapter-3), the minimum film thickness was 0.029 µm, which is less than 0.1 µm. The calculated results also confirmed that the operating lubrication regime at the contact surfaces was in boundary lubrication (Hamrock et al., 2004).

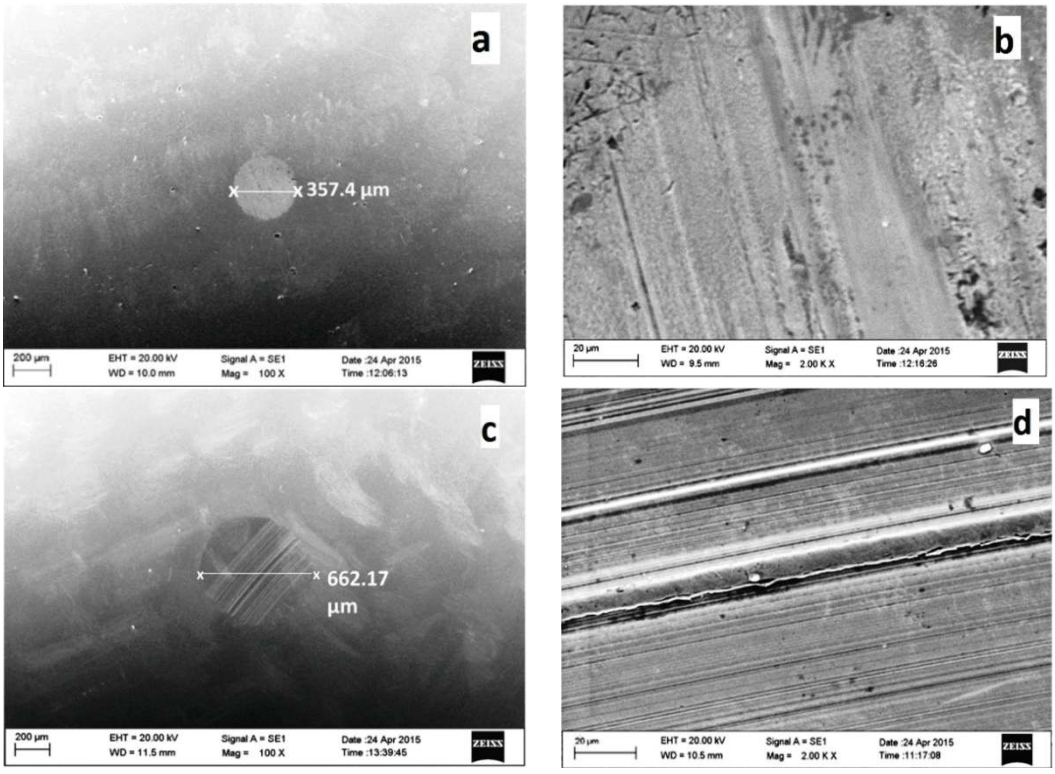

Figure 5.11. SEM images of worn surface (at optimum concentration) lubricated with (a, b) CO+0.25%w/v ZDDP; and (c,d) CO + 0.25%w/v CCTO at different magnification. [Note: a, c at 100x; and b, d at 2000x] (load 392N, speed 1200 rpm for 1hr)

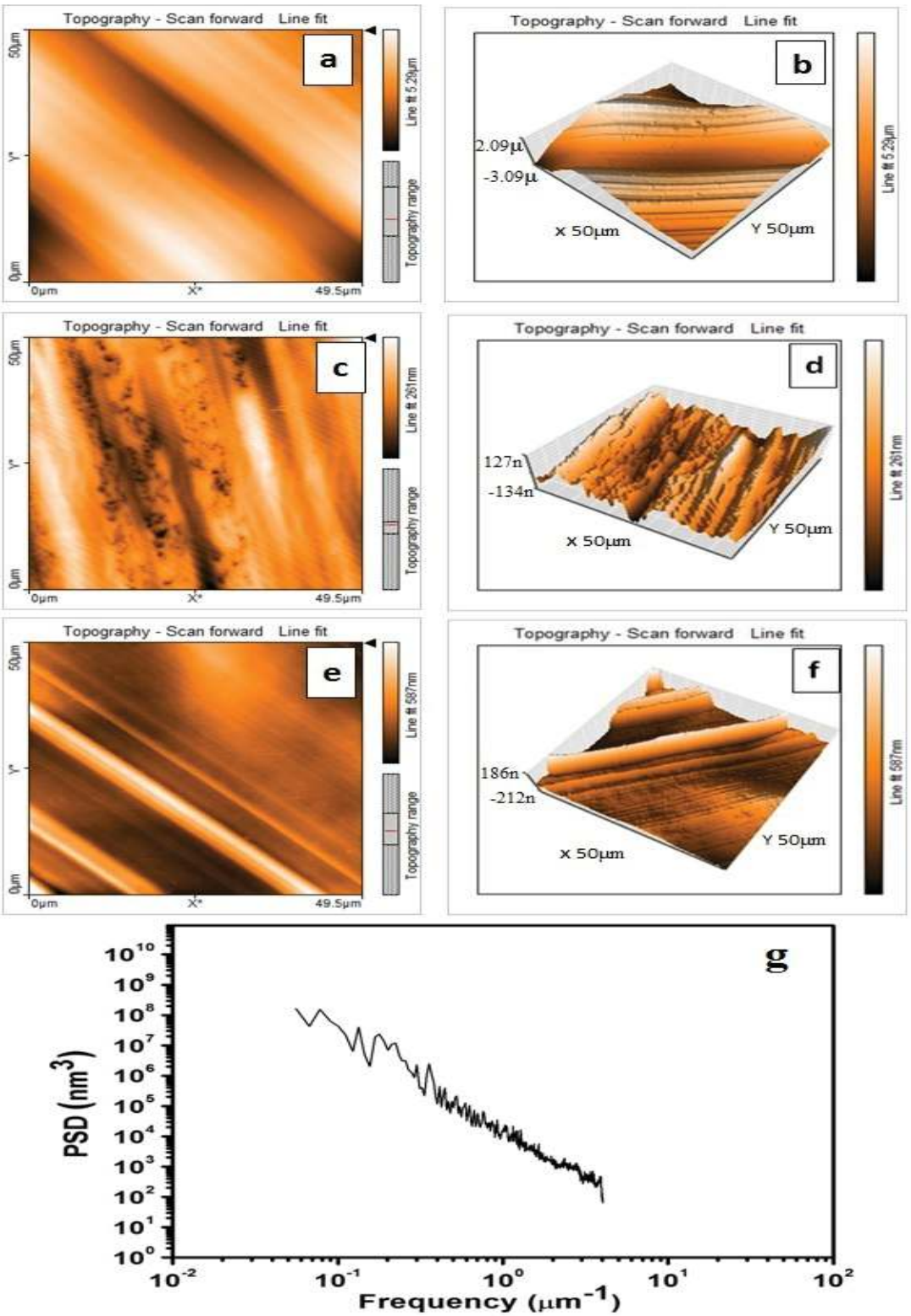

Figure 5.12. AFM images of worn surface lubricated with (a,b) CO, (c, d) CO+0.25%w/v ZDDP(optimum concentration); (e,f) CO + 0.25%w/v CCTO (optimum concentration) at different magnification; and (g) PSD spectrum of worn surface for CO + 0.25%w/v CCTO.

A substantial reduction of surface damage was expected with the use of additives. Root mean square (rms; R_q) roughness values have been reported in our further discussion because it gives representative surface topography of the worn surface.

For paraffin oil compositions, PO revealed the WSD of 670.3 μm, while for additive based PO nanolubricants showed the variation in WSD with the concentration change. As per Table 5.2, it is clear that at all the concentration of ZDDP, WSD was improved significantly and lowest wear at 1.0%w/v of ZDDP. However, CCTO based PO nanolubricant has shown lowest WSD with 0.25%w/v amount, i.e. 413.1μm. Further, increase in the concentration beyond 0.25%w/v the antiwear property started to deteriorate. Thus the concentration 1.0 and 0.25%w/v was assumed to be optimum in PO with ZDDP and CCTO, respectively and presented in Figure 5.13.

SEM and AFM images (Figure 5.12 and 5.14) elucidate that ZDDP in both the base oil, as an additive, revealed smoother worn surfaces as compared to the CCTO nano-additive based oils at optimum concentrations. However, high surface roughness and ploughing marks, observed in case of raw CO and PO. Table 5.3 enumerates the line and area roughness values for different compositions of the nano-additive based lubricants. Roughness results show good agreement with the WSD variation.

Figure 5.15 shows the elemental analysis of the worn steel ball surfaces tested with ZDDP and CCTO particles. These worn surfaces were obtained from the antiwear test. Probably ZDDP forms a strong protective film on the mating surfaces resulting in the wear reduction. Figure 5.15a indicates the presence of Zn, P, S (elements of ZDDP) along with other elements of balls, whereas Figure 5.15b shows the presence of Ca, Ti, Cu (elements of

CCTO) along with the peak of iron. For CCTO nanolubricants the CCTO nanoparticles might have acted as third body interaction between the mating surfaces. Also due to the action of rolling-sliding these hard particles might have been broken and entrapped in the softer steel balls.

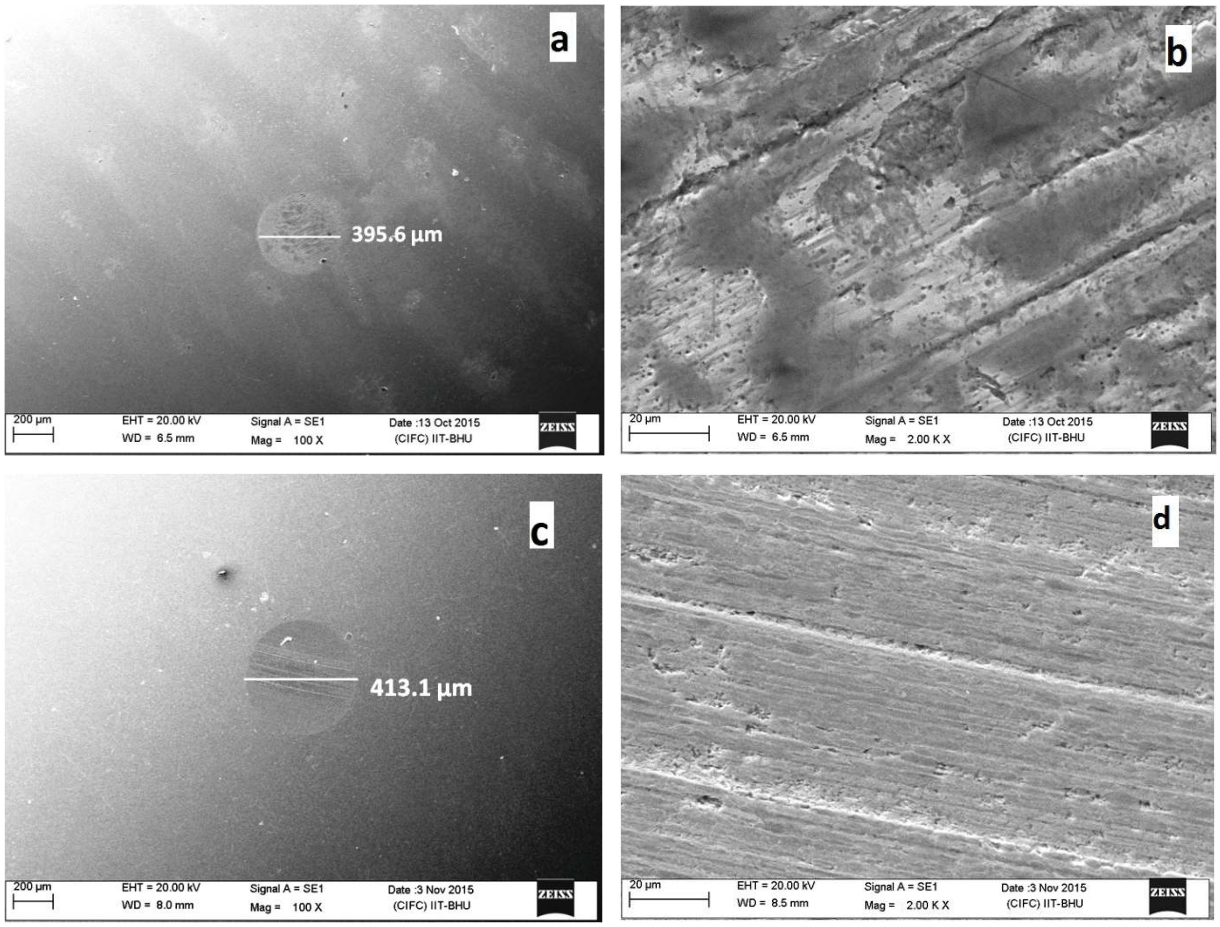

Figure 5.13. SEM images of worn surface (at optimum concentration) lubricated with (a, b) PO+1.0%w/v ZDDP; and (c,d) PO + 0.25%w/v CCTO at different magnification. [Note: a, c at 100x; and b, d at 2000x] (load 392N, speed 1200 rpm for 1h)

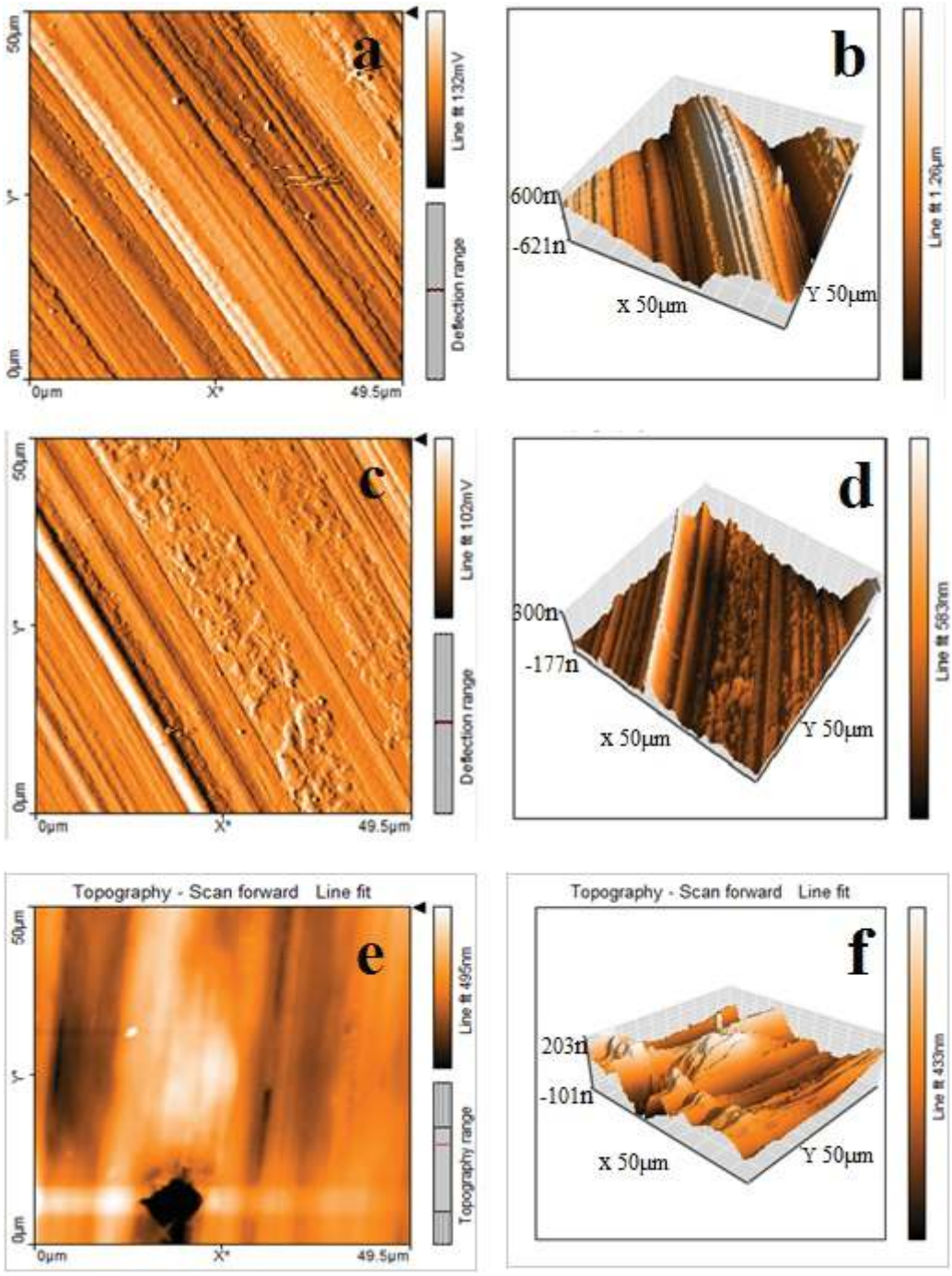

Figure 5.14. AFM images of worn surface lubricated with (a,b) PO, (c, d) PO+0.25%w/v CCTO (optimum concentration); and (e,f) PO + 1.0%w/v ZDDP (optimum concentration) at different magnification. [Note: a, c,e: 2-dimentional; b, d, f: 3-dimensional images, load 392N, speed 1200 rpm and test time 1h]

Table 5.3. Worn surface roughness for different additive based CO and PO compositions.

Oil composition	Line roughness (R_q) (nm) (for 35.3 µm)	Area roughness (S_q) (nm) (For 2500 µm^2)	Oil composition	Line roughness (R_q) (nm) (for 35.3 µm)	Area roughness (S_q) (nm) (For 2500 µm^2)
CO	398.5	393.7	***PO***	347.2	304.5
0.1CZ	55.1	54.3	***0.1PZ***	101.1	103.2
0.25CZ	53.6	47.0	***0.25PZ***	98.3	97.6
0.5CZ	63.4	54.1	***0.5PZ***	68.3	62.8
1.0CZ	102.0	88.6	***1.0PZ***	47.4	51.5
0.1CC	690.1	652.2	***0.1PC***	93.5	101.7
0.25CC	87.9	102.2	***0.25PC***	90.05	92.9
0.5CC	204.1	177.5	***0.5PC***	203.7	201.8
1.0CC	281.4	302.5	***1.0PC***	230.9	214.2

5.3.1.1.1. Discussion

The presence of ZDDP in the base oils reduced the WSD significantly by physisorption and chemisoprtion mechanism. Since ZDDP is completely soluble in the base oils, therefore it alters the intrinsic property of the base oil. Thus increase the interaction between oil molecules and mating surfaces. The improvement in antiwear behavior with ZDDP additive was obtained because ZDDP tends to get adsorbed on the mating surfaces results in the formation of the tribofilm rapidly. The tribo-film form by the ZDDP was layered and complex in nature. In detail, this tribo-film is the combination of sulphides and oxides close to the sample surface, which further covered by long and short polyphosphate chain. The

breakdown products of ZDDP have a critical role in tribo-film formation which results in enhanced tribological characteristics (Stachowiak, 2005).

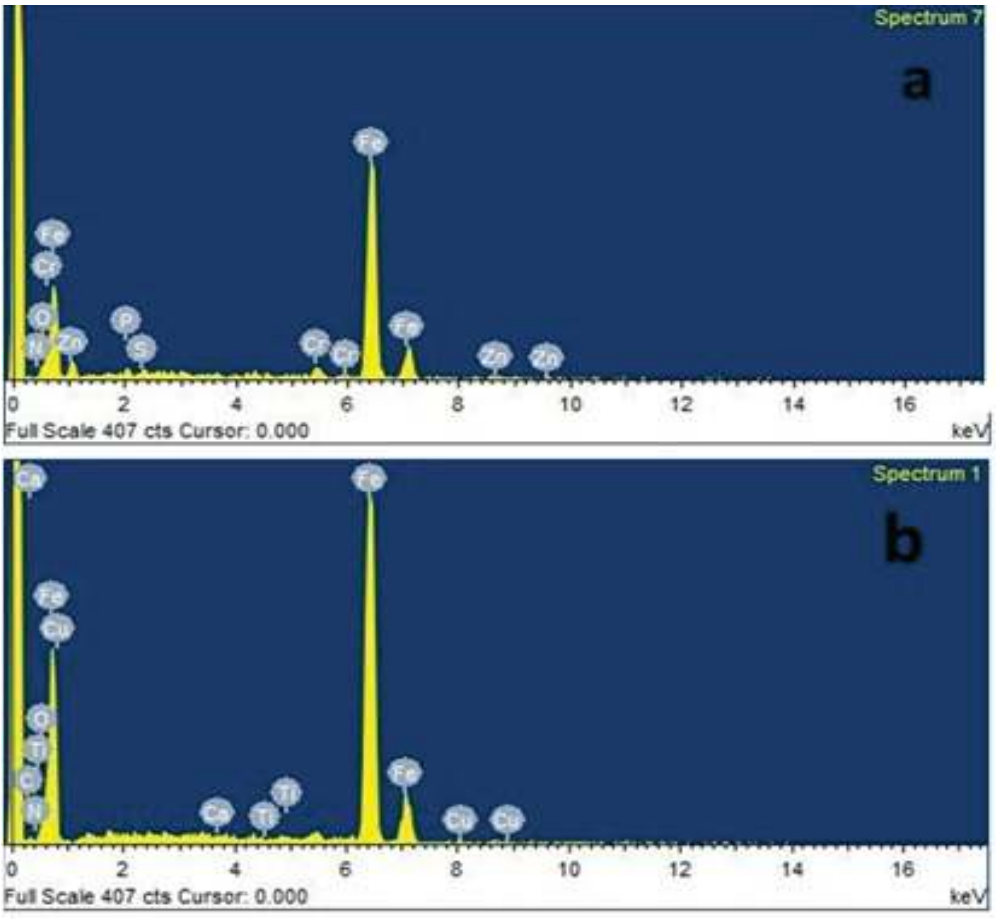

Figure 5.15. Typical EDS spectrum of worn surfaces tested with (a) ZDDP and (b) CCTO compositions.

For the nanoparticle based lubricants, the improvement in tribological behavior may involve one or more in-situ mechanisms. The two probable reasons for enhanced tribological behavior may be (i) the rolling, sliding or combined action of nanoparticles in contact zone and (ii) the reduction in the real area of contact. It can be speculated that the variation in the size of nanoparticles directly affects the nanolubricant performance. In other words, the

smaller nanoparticles fill the micro-pits and valleys at the contacting interface, and the bigger one separates the asperities (Lovell et al. 2010). Figure 5.16 represents a typical interaction of contacting surfaces and probable in-situ phenomena in the presence of a lubricant. At the application of the load, the nanoparticles may distort to some extent which causes a minute increment in the area of contact between nanoparticles and the rubbing surfaces (Figure 5(a)). In spite of this, the real contact area is too low as compared to the nominal area (Ghaednia and Jackson, 2013). In case of mating surfaces lubricated with the base oils without nano-additives, the metal to metal interaction is predominant. The asperity-asperity collision causes adhesive wear of material and local heat may be generated (Figure 5.16(b)).

On the contrary, in the case of mating surfaces lubricated with nanolubricants, the interaction of metal-metal can alter to dominating metal-ceramic at the interface. Kong et al. (2017) reported that the asperities/peaks have higher surface energy than the valleys from the definition of solid surface energy. Thus the majority of the nanoparticles tends to deposit on the asperity and generates a new film i.e. “protective film of the nanoparticles”. It supports in reduction of real contact area between the contacting surfaces (Figure 5.16(c)). Also, some nanoparticles get deposited in the valleys to smoothen the interface. Another phenomenon may associate with the nanolubricants (Figure 5.16(c)) is a nano-bearing effect or simply rolling mechanism of the nanoparticles. Also, each ball has experienced a huge contact pressure and it was typically 3.402 GPa (Gupta and Harsha 2017). Therefore, there is a chance of embedment of the nanoparticles into the comparatively softer ball surface. The rolling mechanism of the nanoparticles between mating surfaces occurs only when harder nanoparticles passed over the embedded nanoparticles (Kong et al. 2017; Khadem et al. 2016).

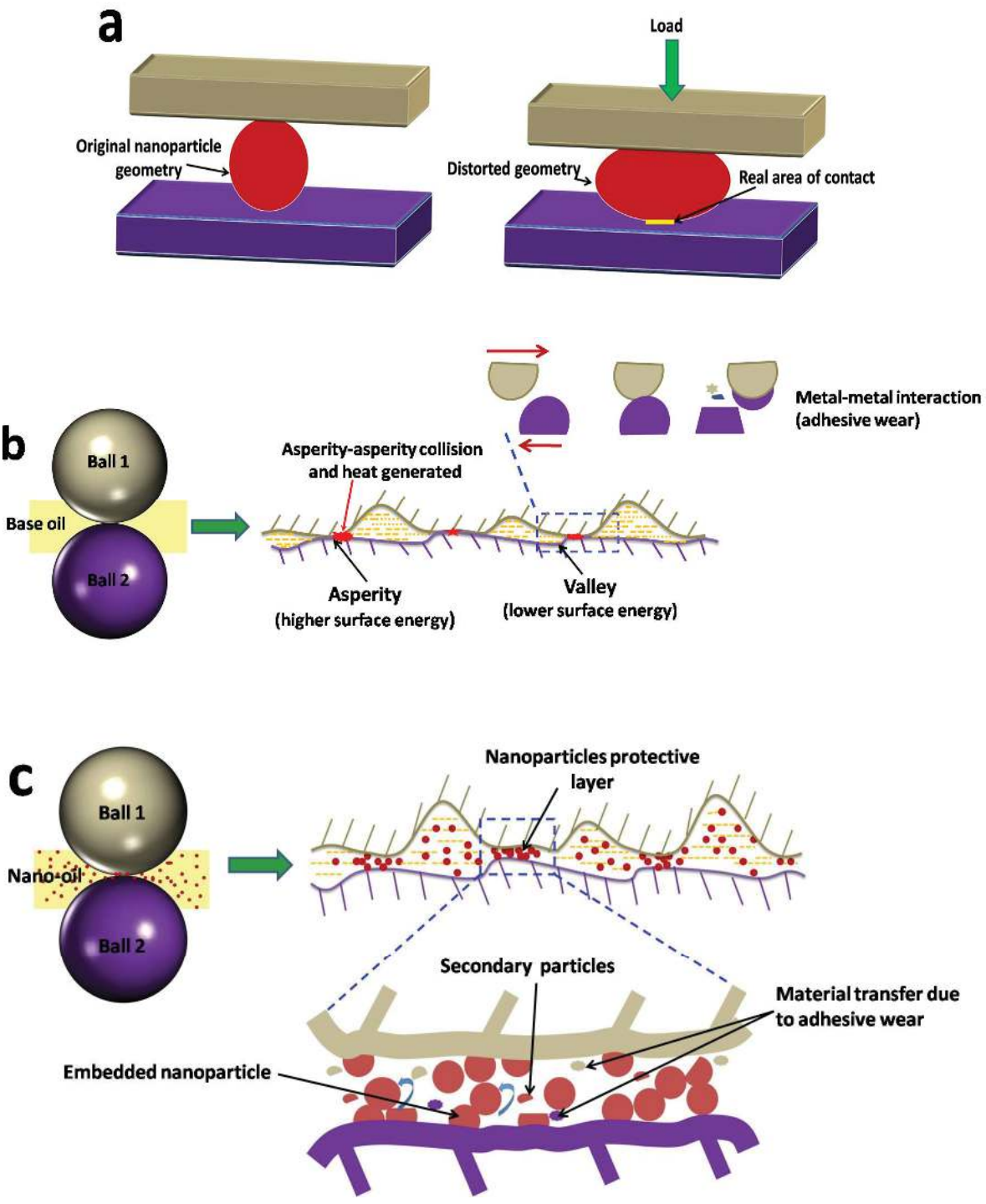

Figure 5.16. Possible in-situ phenomena for the lubricated sliding contacts; (a) reduction in real contact area, (b) lubrication with base oil and (c) synergistic interaction of nanolubricant-surface.

Wäsche et al. (2015) also reported that during sliding secondary tiny particles are generated from the self-wear of the top surface of the nanoparticles by micro-shearing, which directly help in surface mending to achieve improved tribo-performance.

It is important to note that the improvement in the tribo-performance for nanolubricants is not necessary to follow the same lubrication mechanism for all the solid nano-additives. Xie et al. (2016) distinguished the lubrication mechanisms between the oxide based nanoparticles in base oil and solid lubricants (i.e., MoS_2, WS_2, graphite etc.). They pointed out that the particle structure and their behavior at a high contact temperature and pressure differentiate the lubrication mechanism. Solid lubricants have mostly layered structure with a stable interlayer covalent bond; on contrary oxide nanoparticles are crystalline and hard. Thus, the lubrication mechanism of MoS_2, WS_2 like solid lubricants reflected by the shearing of molecular layers and formation of transfer film (Vladimir et al. 2014), in contrast, oxide nanoparticles deals with the formation of nanoparticle protective film, mending, rolling-sliding, polishing, etc. Oxide nanoparticles can effectively work at higher operating temperature and pressure, whereas solid lubricants show inferior tribo-performance.

5.3.1.2. Antifriction study

Figure 5.17 depicts the variation in average COF with concentration and Table 5.4 reports the summary of average COF and interfacial shear stress for different oil compositions. Additive based lubricants have shown a reduced COF than the base oils. However, as the additive content increasing then COF increased linearly. For PO compositions, the minimum COF was obtained at 0.25 and 1.0%w/v for CCTO and ZDDP additives, respectively. However, CCTO with CO has improved the friction property with 0.1%w/v concentration. Also, COF

increases with concentration, and shows highest friction value even more than the base CO at 1.0%w/v concentration. It is noticeable that ZDDP friction property was deteriorated with CO, while improvement was observed with PO for all the concentrations. The hydroxyl functional group in CO reduces the rate of chemisorption reaction with ZDDP at the mating surfaces, while PO has no such ability because of the straight hydrocarbon chain. Sharma et al. (2009) argued that the hydroxyl functional group (polar) of CO attracts the oil molecules rapidly than non-polar oil and it gets adsorbed on the mating surfaces. ZDDP decomposes during frictional heating and forms an amorphous region of short-chain polyphosphates and thiophosphates, with longer chain polyphosphates in the outer region. However, the more polar nature of CO dominates over these long and short chain glossy films (Hutchings et al., 2016). Thus, a decomposition product of ZDDP adsorbs on the mating surface at a very low rate. Therefore, highest concentration of ZDDP in PO reveals lowest mean COF; on the contrary, CO exhibits higher mean COF.

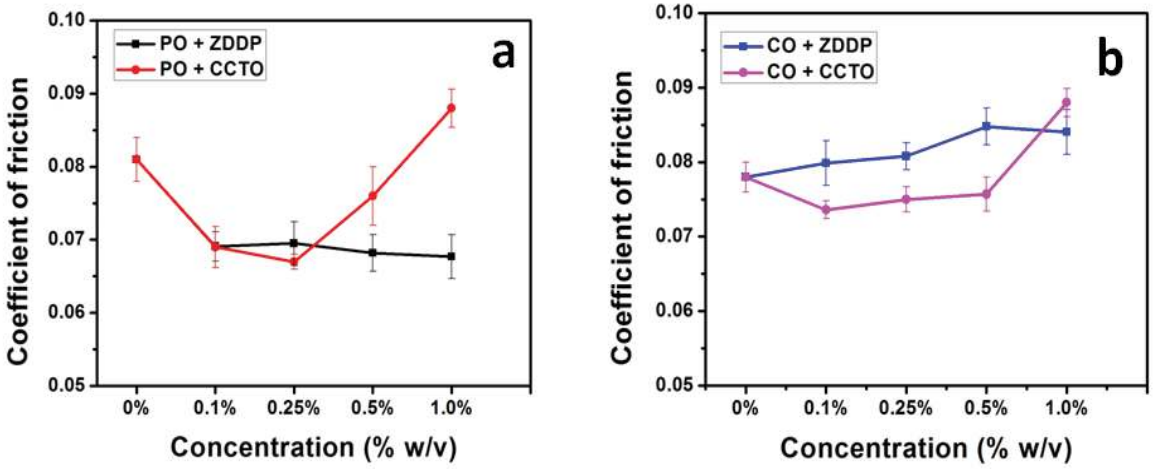

Figure 5.17. Variation in average COF for (a) PO and (b) CO compositions tested at 392N load for 1h.

The COF trend for CCTO based nanolubricants exhibits a critical role of the reduction in the real contact area (Ghaednia et al., 2013). The lower concentrations of nanoparticles was

sufficient to achieve the minimum coefficient of friction, beyond which nanoparticles might have acted as abrasive agents giving rise to three body abrasion phenomenon. The optimum concentration of nanoparticles in the lubricant for good tribological performance may be get effected with the type of contact configuration (i.e. a point or surface contact) and loading condition. The higher number of nanoparticles might be needed to reduce the real area of contact for the surface contact than in a point contact.

Table 5.4. Average COF and interfacial shear stress for ZDDP and CCTO additive based CO and PO compositions. (σ: standard deviation for COF)

Oil composition	COF (Avg.)	σ	Interfacial shear stress (MPa)	Oil composition	COF (Avg.)	σ	Interfacial shear stress (MPa)
CO	0.078	0.0037	158.6	***PO***	0.081	0.0051	164.7
0.1CZ	0.07987	0.002	162.5	***0.1PZ***	0.0691	0.0062	140.5
0.25CZ	0.0808	0.0033	164.3	***0.25PZ***	0.0695	0.0031	141.3
0.5CZ	0.0848	0.005	172.4	***0.5PZ***	0.0682	0.0029	138.7
1.0CZ	0.0840	0.0049	170.8	***1.0PZ***	0.0677	0.007	137.7
0.1CC	0.0736	0.0061	149.7	***0.1PC***	0.069	0.0043	140.3
0.25CC	0.075	0.0023	152.5	***0.25PC***	0.067	0.0019	136.2
0.5CC	0.0757	0.0024	153.9	***0.5PC***	0.076	0.0055	154.5
1.0CC	0.088	0.0041	178.9	***1.0PC***	0.088	0.0048	178.9

Interfacial shear stress was obtained by the multiplication of COF with flow stress of the material. It represents the response of the mating surfaces at the interface. Lower values of the interfacial shear stress indicate good lubrication potential of the oil and also act as a friction modifier. In case of CO compositions, ZDDP did not show any improvement in interfacial stress, while it was reduced for CCTO amount of 0.1%w/v. On the contrary, for

PO compositions interfacial stress was reduced substantially for both ZDDP and CCTO nanolubricants. The interfacial shear stress varied with similar trend of COF because of direct proportional relation.

5.3.1.3. Extreme-pressure (EP) study

EP test shows weld load performance of the lubricant by evaluation of the catastrophic failure of the film. The typical image of welded ball is presented in Figure 5.18. And, the tested load just before the weld load is called as last non-seizure or pass load. Table 5.5 summarized the pass load and weld load capacity of the lubricants for all the composition with ZDDP and CCTO. Since the duration of EP test was only 10 seconds as per the ASTM standard and loading condition continuously increasing with each new test. Therefore, the formation of the protective film reflects the EP behavior of any lubricant.

For base CO and PO, the last non-seizure and weld load was observed at 126 and 160 kgf respectively. The lower concentration ranges (up to 0.25%w/v) of the additives have no effect on the EP property. Up to 0.25%w/v concentration, both the additives behave similarly to the base oils. The ZDDP have shown similar weld load capacity for both the base oil. The highest pass load and weld load for ZDDP was obtained with 1.0%w/v amount, which was 200 and 250 kgf respectively. However, highest pass load for CCTO nanoparticles based lubricants was 160 kgf while weld loads as 200 kgf.

Probably, at low concentration of ZDDP thick tribo-film was not formed to sustain the higher applied load, while at higher concentrations it is possible. However at lower CCTO concentrations (0.1 and 0.25 %w/v), the number of particles was not sufficient to stay at contact zone. This is because under higher load and speed the particles may squeeze out thus similar EP performance as base oils. As the concentration increased the threshold number of

particles may available even after squeezing-out action and keep the asperities away. Laura et al. (2014) also argued the similar load carrying performance for different nanofluids.

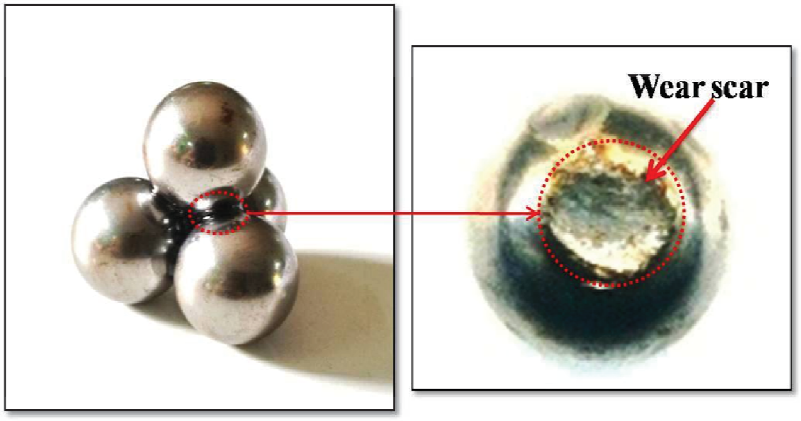

Figure.5.18. Optical image of heavily worn surface of detached welded ball.

Table 5.5. Summary of EP behaviour for different additive based CO and PO compositions.

Oil composition	Last non-seizure load (kgf)	Weld load (kgf)	Oil composition	Last non-seizure load (kgf)	Weld load (kgf)
CO	126	160	***PO***	126	160
0.1CZ	126	160	***0.1PZ***	126	160
0.25CZ	126	160	***0.25PZ***	126	160
0.5CZ	160	200	***0.5PZ***	160	200
1.0CZ	200	250	***1.0PZ***	200	250
0.1CC	126	160	***0.1PC***	126	160
0.25CC	126	160	***0.25PC***	126	160
0.5CC	126	160	***0.5PC***	160	200
1.0CC	160	200	***1.0PC***	160	200

5.3.2. Evaluation of tribo-performance for S-CuO based lubricants

During the suspension stability test by visual inspection, it was observed that unmodified CuO particles start to settle down at the bottom of the jar rapidly after the sample preparation. This may due to a bigger size range of the CuO nanoparticles. However, surface treated S-CuO has shown good suspension stability for a prolonged time. Therefore, S-CuO nanoparticles were used in this study as nano-additive in various biolubricants, i.e. castor oil (CO), rapeseed oil (RO), sunflower oil (SO). Also, tribo-performance was compared with the paraffin oil (PO).

5.3.2.1. Antiwear study

On the basis of antiwear results, WSD for different oil compositions are summarized in Table 5.6. In the latter part of our discussion, PCu, CCu, RCu and SCu referred as nanolubricant compositions having S-CuO nanoparticles in PO, CO, RO and SO respectively. Prefix 0.1, 0.25, 0.5 and 1.0 enumerate the concentration (%w/v) of nano-additives. Figure 5.19 and 5.20 depicts the SEM images of the worn surfaces with the use of raw PO, CO and RO, SO respectively at different magnifications. And, Figure 5.21 and 5.22 represents the S-CuO based nanolubricants including the optimum concentrations for different selected oils at different magnifications. The worn surfaces reveal that the WSDs observed for CO (i.e. 906.4 μm), RO (788.4 μm), SO (873 μm) were higher than PO (i.e. 670.3 μm). For the base oils, the surface deterioration and trench-like appearance indicate the simultaneous action of micro-ploughing and micro-cracking along with the adhesion. It is speculated that the CO might have weak adherence ability in spite of the presence of hydroxyl functional group and shows similar ease migration property like silicone oil (Zhou et al., 2009). However, RO and

SO has inferior and slow tribo-film formation rate, which cause severe were of the mating balls.

Table 5.6. Summary of WSD, wear reduction (WR), and mean wear volume (MWV) for different concentration of S-CuO with PO, CO, RO and SO.

Oil compositions	WSD (µm)	WR (%)	MWV (x10^{-4} mm^3)
PO composition			
PO	670.3	…	28.42
0.1PCu	644.5	3.84	23.9
0.25PCu	664.7	0.84	27.4
0.5PCu	668.0	0.34	28.0
1.0PCu	521.5	22.2	9.3
CO composition			
CO	906.4	…	100.5
0.1CCu	688.5	24.04	31.9
0.25CCu	773.4	14.67	52.1
0.5CCu	817.4	9.82	65.6
1.0CCu	922.9	-1.82	108.3
RO composition			
RO	788.4	…	56.4
0.1RCu	710.8	9.84	36.5
0.25RCu	861.4	-9.26	81.5
0.5RCu	1052.1	-33.45	185.1
SO composition			
SO	873.0	…	86.1
0.1SCu	888.1	-1.73	92.5
0.25SCu	993.2	-13.76	146.3
0.5SCu	856.9	1.84	79.8
Negative sign indicates impaired antiwear property.			

The formulated nanolubricants have shown significant improvement in the WSD. On the basis of improved antiwear results, the different oil compositions were ordered as follows:

For formulated PO: $1.0PCu < 0.1PCu < 0.25PCu < 0.5PCu < PO$

For formulated CO: $0.1CCu < 0.25CCu < 0.5CCu < CO < 1.0CCu$

For formulated RO: $0.1RCu < RO < 0.25RCu < 0.5RCu$

For formulated SO: $0.5SCu < SO < 0.1SCu < 0.25SCu$

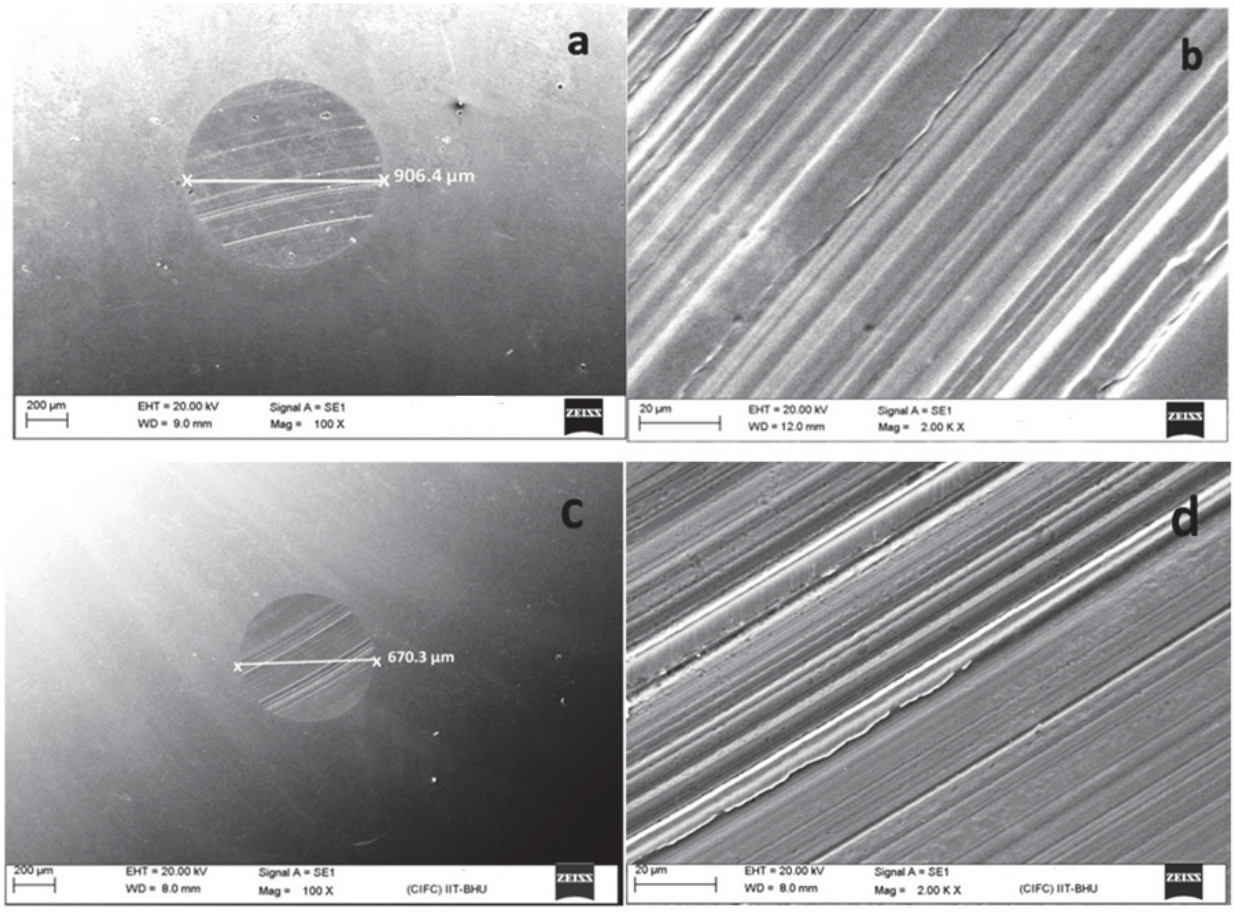

Figure 5.19. SEM image of worn steel balls with (a,b) CO; (c,d) PO [Note: load 392N, speed 1200 rpm, time 1h; a and c at 100x ; b and d at 2000x]

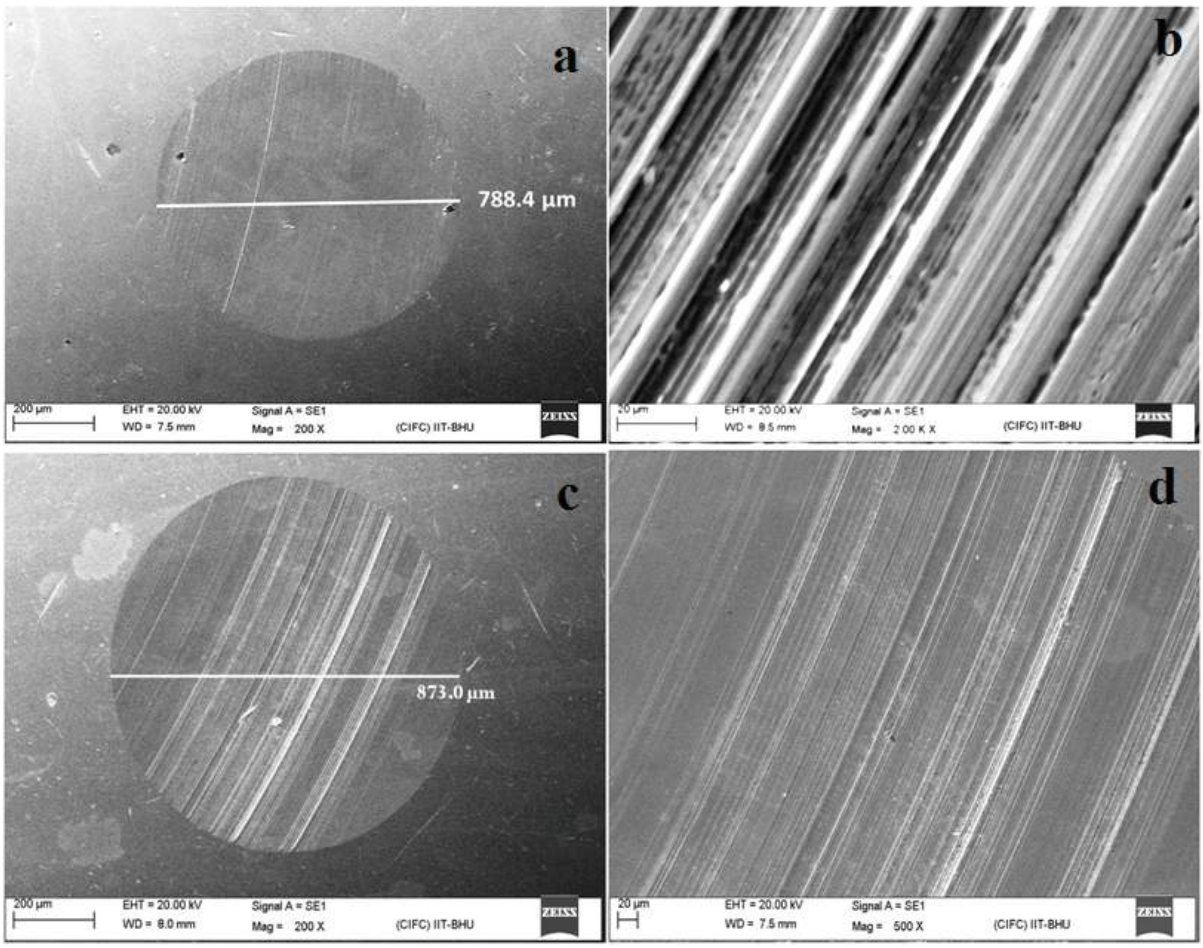

Figure 5.20. SEM images of worn steel balls (at different magnification) tested at load 392N for 1h with (a,b) RO; (c,d) SO.

SEM micrographs of the worn surfaces for formulated oils show mostly smooth areas representing low wear regime. However some part shows initiation of severe wear, it may due to the materials overload and generation of crack due to fatigue (Wäsche et al., 2015). Also, particle size variation affects the tribological test results. Lovell et al. (2010) reported that the ultrafine particles exhibits mending effect and smoothen the rubbing surfaces. However, bigger size nanoparticles participate in carrying fractional applied load. Both of these actions provide lower interfacial shear stress. The WSD varied between 2.4 to 5.9% for different compositions of oils.

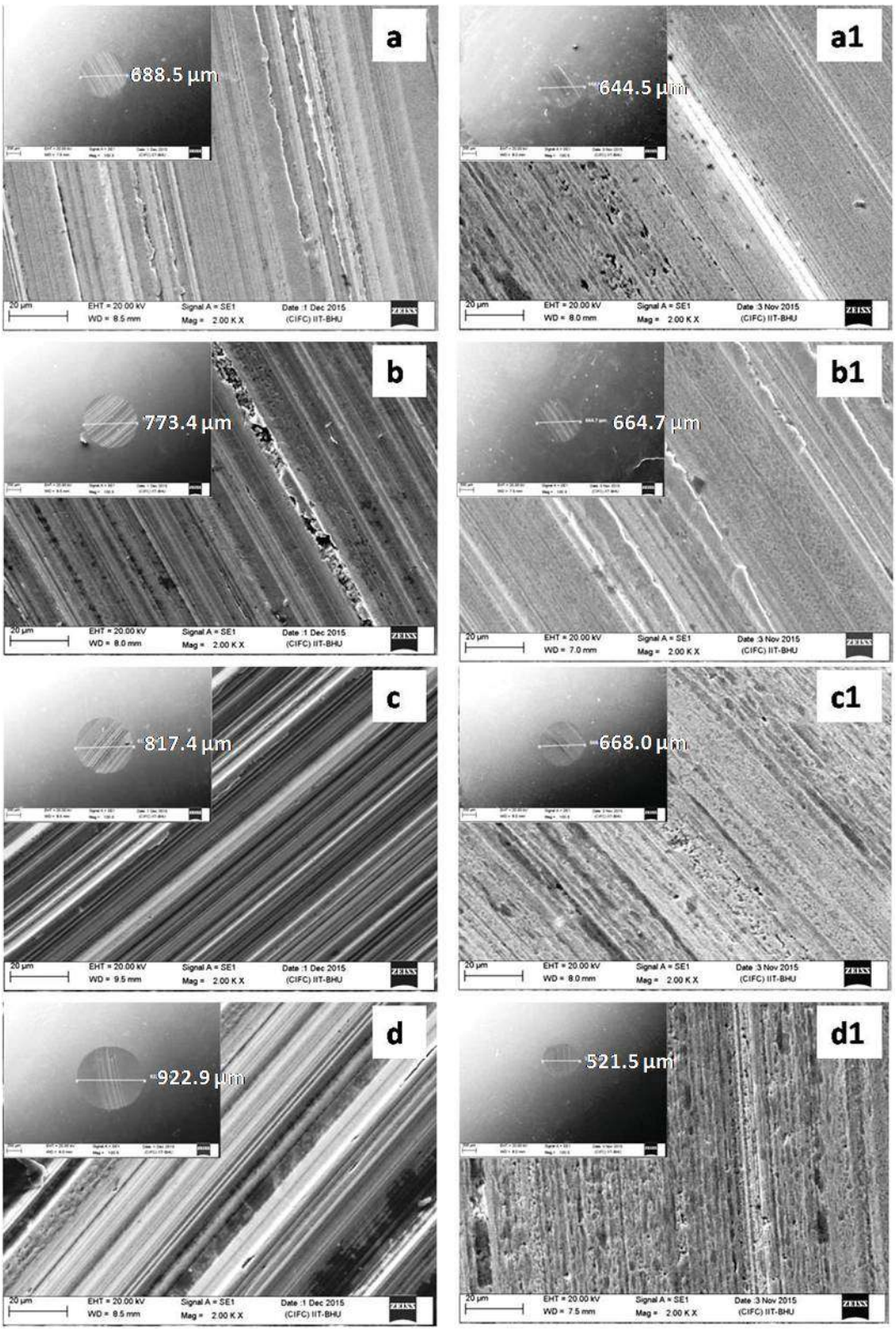

Figure 5.21. Micrograph of worn steel balls with (a) 0.1CCu, (b) 0.25CCu, (c) 0.5CCu, (d) 1.0CCu (a_1) 0.1PCu, (b_1) 0.25PCu, (c_1) 0.5PCu and (d_1) 1.0PCu. (load 392N, speed 1200 rpm, time 1h)

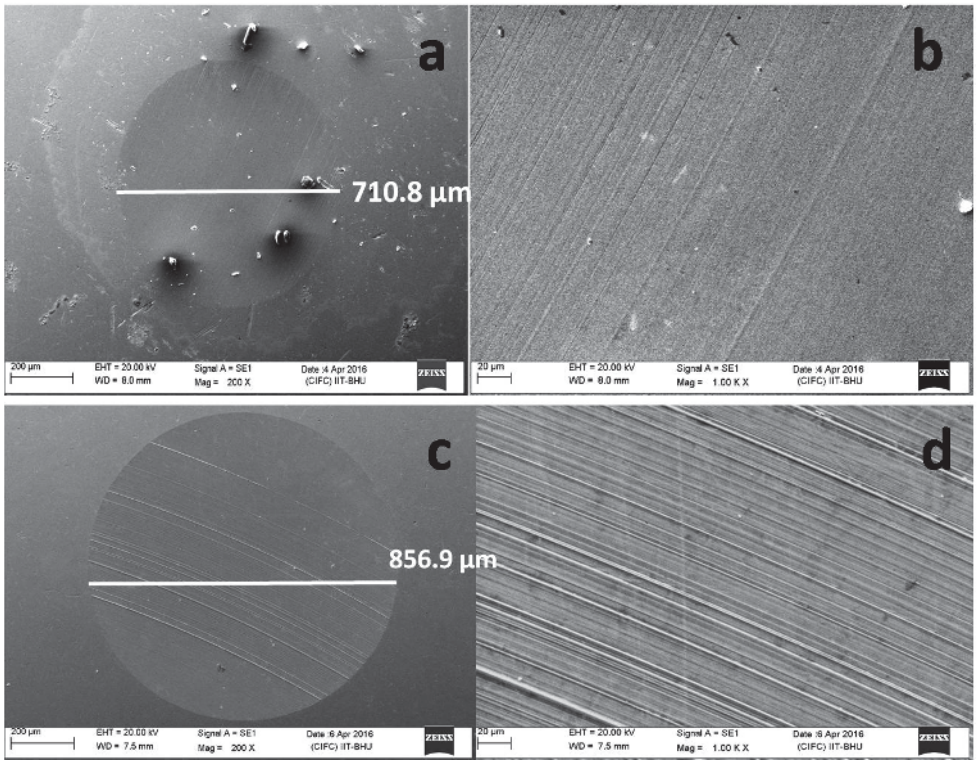

Figure 5.22. Micrograph of worn steel balls at optimum concentrations; (a, b) 0.1RCu, (c, d) 0.5SCu at different magnifications. (load 392N, speed 1200 rpm, time 1h)

From lowest WSD, antiwear results conclude that 1.0PCu, 0.1CCu and 0.1RCu were noticed to be optimum compositions for PO, CO and RO respectively (Table 5.6 and Figure 5.21-5.22). However, SO did not show any substantial improvement in antiwear property with S-CuO. Although minute WSD reduction was observed for 0.5SCu, however it cannot be considered as optimum composition. A close observation reveals a drastic fluctuation in the WSD for CO and RO compositions as compared to PO compositions with a small variation in concentration. It indicates a strong concentration sensitive behavior of formulated CO and RO. This may be due to the presence of polarity and a functional group in the vegetable oils and hydrogen bond between functional group molecules and SDS as well (Sui et al., 2016).

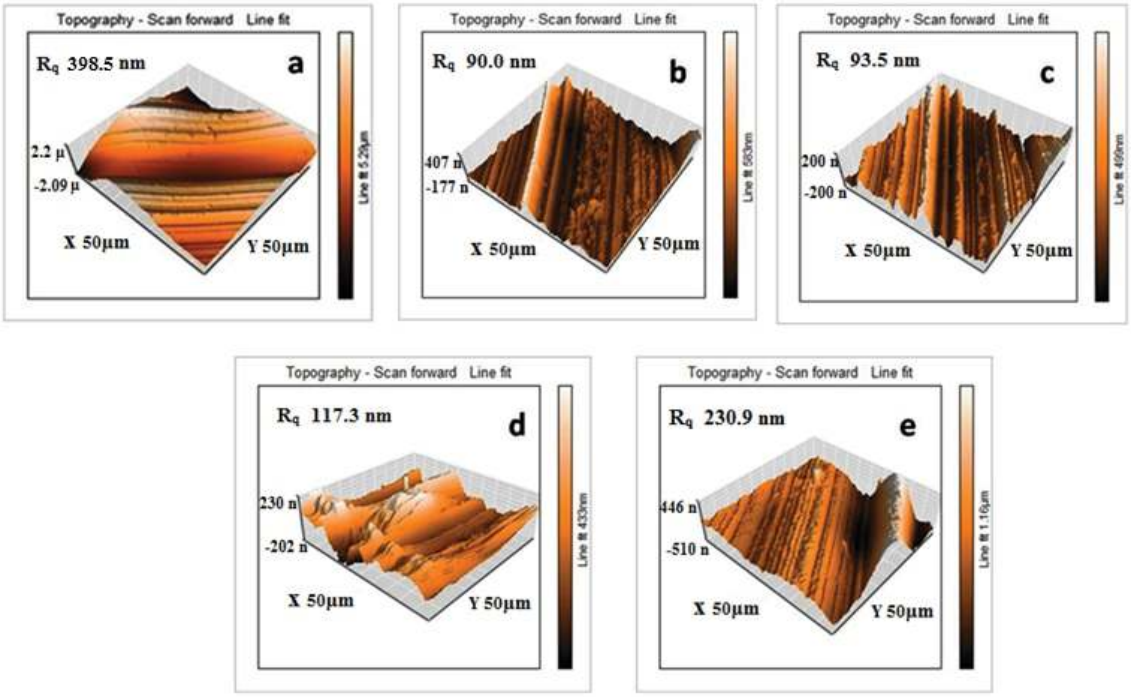

Figure 5.23. AFM roughness images of worn surfaces for different CO compositions; (a) CO, (b) 0.1CCu (c) 0.25CCu (d) 0.5CCu and (e) 1.0CCu. [load 392N, sliding speed 1200 rpm, time 1h]

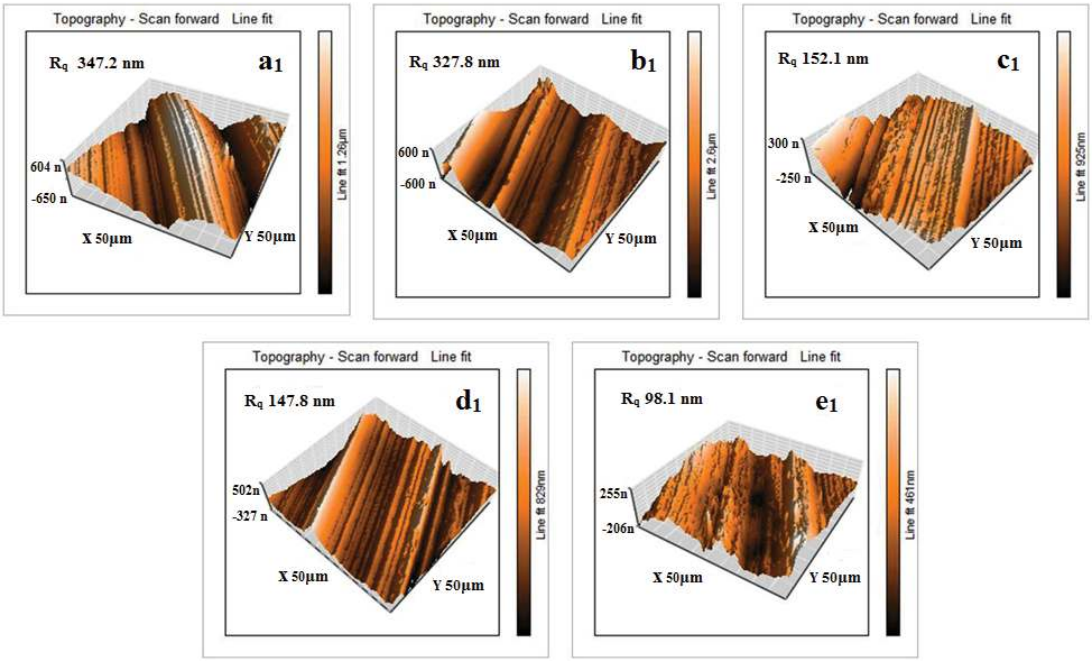

Figure 5.24. AFM roughness images of worn surfaces for different PO compositions; (a_1) PO, (b_1) 0.1PCu (c_1) 0.25PCu (d_1) 0.5PCu and (e_1) 1.0PCu. [load 392N, sliding speed 1200 rpm, time 1h]

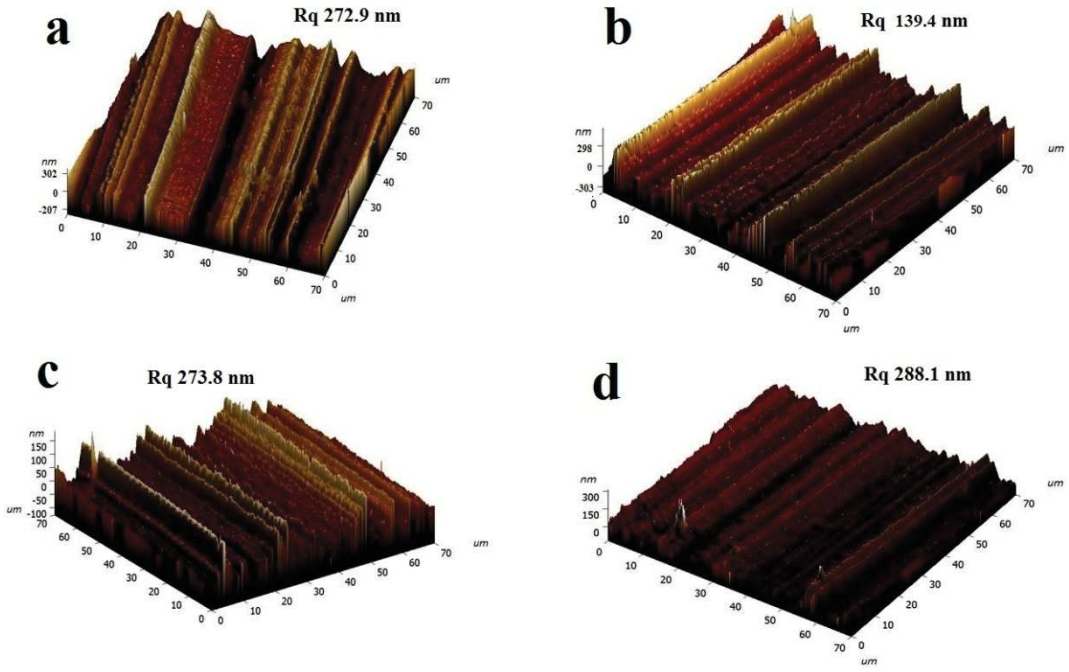

Figure 5.25. AFM roughness images of worn surfaces for different RO compositions; (a) RO, (b) 0.1RCu (c) 0.25RCu, and (d) 0.5RCu. [load 392N, sliding speed 1200 rpm, time 1h]

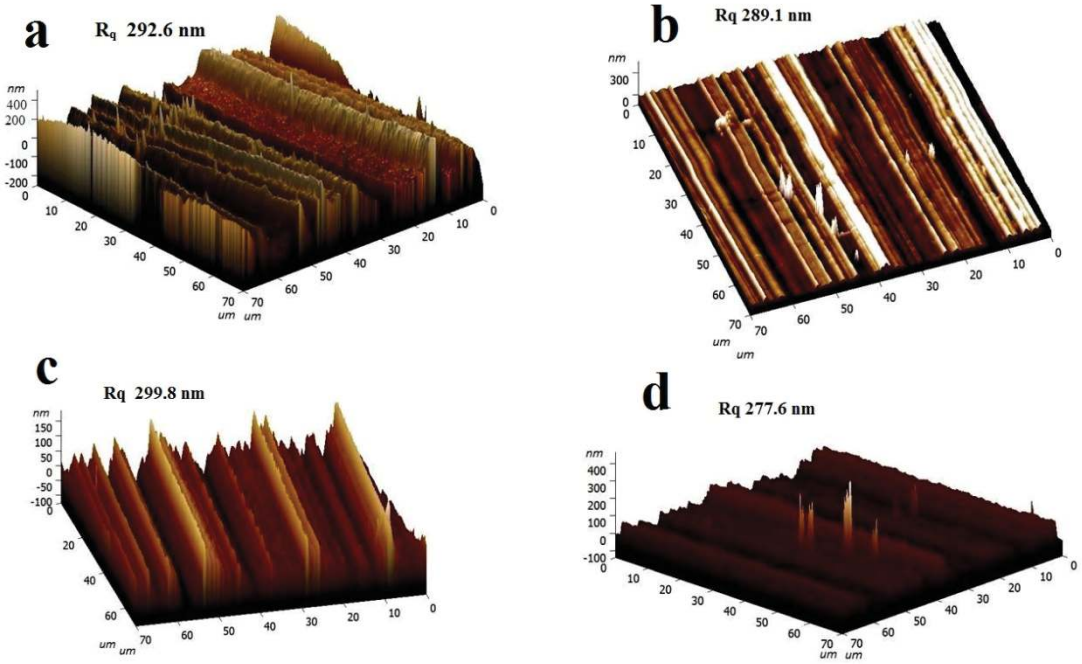

Figure 5.26. AFM roughness images of worn surfaces for different SO compositions; (a) SO, (b) 0.1SCu (c) 0.25SCu, and (d) 0.5SCu. [load 392N, sliding speed 1200 rpm, time 1h]

Figure 5.23 – 5.26 represents the surface roughness of the worn track tested with CO, PO, RO and SO with its all compositions respectively. The surface roughness property shows analogous relation as WSD variation with the change in concentration. It reflects that the modified S-CuO nanoparticles in CO and RO (polar in nature) uniformly dispersed as per the similarity principle. According to the similarity principle, the substance with similar nature is most likely to be attached or dissolved by each other (Yan et al. 2014). As it is known that the SDS has a polar head and a non-polar tail. This polar head easily attached with the molecules of the oil (polar in nature) and non-polar tail with the nanoparticle surface. This helps in uniform and prolonged suspension, which reflects on the tribo-performance. Suarez et al. (2010) reported that triglycerides of the biolubricants are more polar than petro-products. Tan et al. (2002) also explained that the effectiveness of any lubricant depends upon persistent interaction between polar end of oil molecules and contacting surfaces. Therefore, the lower concentrations were sufficient to separate the mating surfaces, whereas higher concentration deteriorates the surface by abrasion. The opposite phenomenon observed for PO which is non-polar by nature. In all the cases, the worn surfaces have shown severely furrowed surfaces, which are shreds of evidence for the close contact situation (Ghaednia et al., 2015). The AFM results show that lubricants with varying nanoparticle concentration have influenced the surface roughness significantly. At the optimum concentrations, the maximum reduction in the R_q was noticed. The maximum reduction in roughness for PO composition was 71.4% (at 1.0PCu), for CO compositions 77.4% (at 0.1CCu), for RO compositions 48.9% (at 0.1RCu) and for SO composition it was very low i.e. 5.12% at 0.5SCu. Table 5.6 reveals the highest wear reduction (WR) as 24.04% with the CO composition, i.e. for 0.1CCu. However, for PO, RO and SO compositions the maximum

WSD reduction was 22.2, 9.84 and 1.84% respectively at optimum concentrations. The negative sign in the Table 5.6 exhibits impaired antiwear behaviour with the addition of S-CuO additives. Figure 5.27 and Table 5.6 enumerates mean wear volume (MWV) variation. Also, Figure 5.28 represents specific wear rate calculated for all the lubricants compositions using Archard's law.

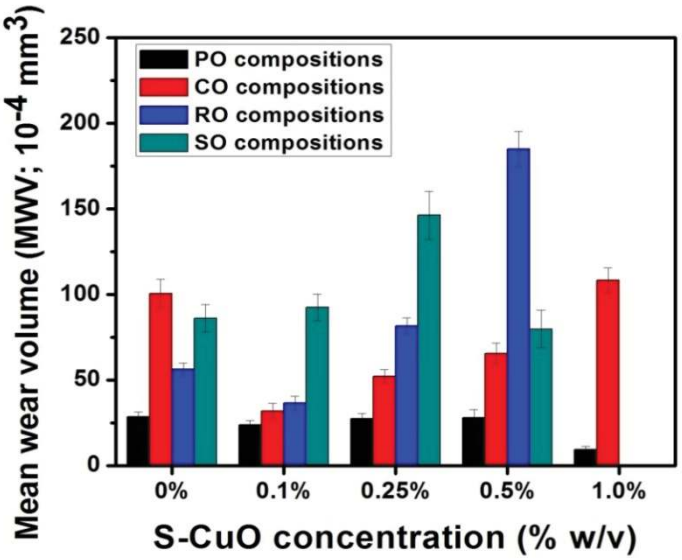

Figure 5.27. MWV of worn surfaces lubricated with different oils with S-CuO nano-additives.

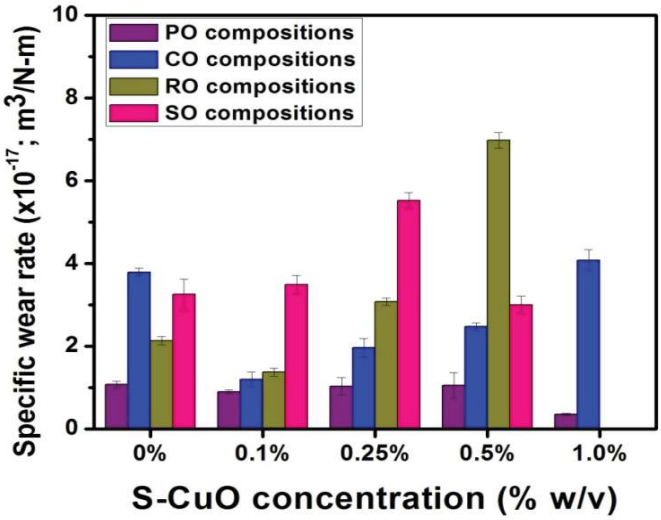

Figure 5.28. Specific wear rate for the worn surfaces lubricated with different oils with S-CuO nano-additives.

Table 5.7.Summary of specific wear rate for different concentration of S-CuO with PO, CO, RO and SO.

Oil compositions	Specific wear rate (m^3/N-m)
PO composition	
PO	1.07×10^{-17}
0.1PCu	0.9×10^{-17}
0.25PCu	1.033×10^{-17}
0.5PCu	1.055×10^{-17}
1.0PCu	0.35×10^{-17}
CO composition	
CO	3.79×10^{-17}
0.1CCu	1.20×10^{-17}
0.25CCu	1.96×10^{-17}
0.5CCu	2.47×10^{-17}
1.0CCu	4.08×10^{-17}
RO composition	
RO	2.13×10^{-17}
0.1RCu	1.37×10^{-17}
0.25RCu	3.074×10^{-17}
0.5RCu	6.98×10^{-17}
SO composition	
SO	3.25×10^{-17}
0.1SCu	3.486×10^{-17}
0.25SCu	5.52×10^{-17}
0.5SCu	3.0×10^{-17}

The calculated MWV indicates that the higher material loss obtained either for the base lubricants or the higher concentration range (0.5%w/v onwards). It show in-line trend with the WSD. This is because MWV was calculated with the help of the WSD in direct proportion (Eq. 3.7). The lowest material loss was, of course, for the worn surfaces lubricated with the optimum concentrations. For PO, CO, RO and SO composition at 1.0, 0.1, 0.1 and 0.5%w/v show the lowest MWV as 9.3, 31.9, 36.5 and 79.8 respectively (Table 5.6).

The variation in specific wear rate for different nanolubricant compositions is presented in Table 5.7. The variation in specific wear rate shows similar tendency as the MWV. For both CO and RO compositions, 0.1%w/v exhibits the lowest specific wear rate, i.e. $1.2x10^{-17}$ and $1.37x10^{-17}$ m^3/N-m respectively, while without additive these oils gave the specific wear rate values as $3.79x10^{-17}$ and $2.13x10^{-17}$ m^3/N-m respectively. After this concentration linear increment in specific wear rate was observed. It may be expected that at higher concentrations more solid to solid contacts, whereas, solid to liquid contacts are pronounced with lower concentrations (Ghaednia and Jackson 2013). On the contrary, it was also observed that as the S-CuO content increased in PO and SO, the specific wear rate increased linearly and sudden decreased at highest optimum concentrations i.e., 1.0PCu and 0.5SCu.

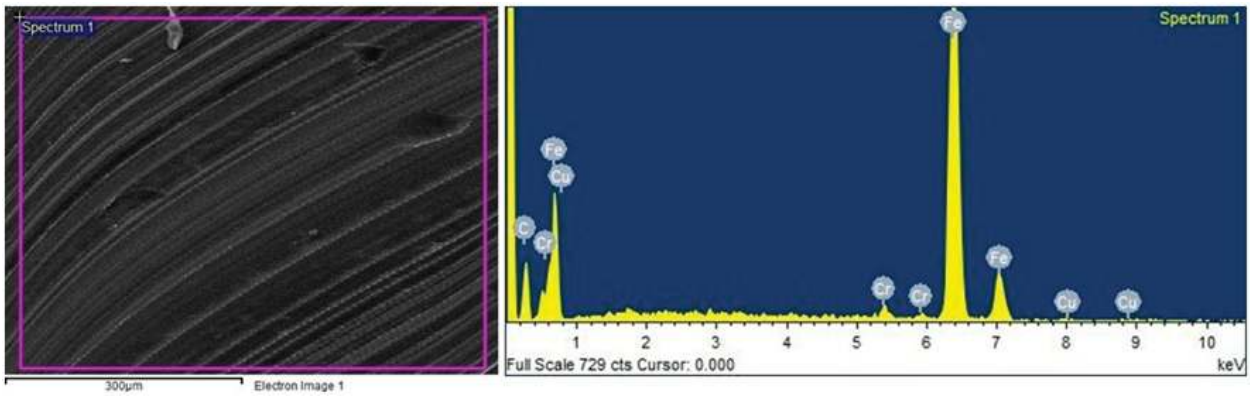

Figure 5.29. Typical chemical elemental analysis of worn surface for 0.1CCu.

Typical elemental analyses of the worn surfaces were presented in Figure 5.29. The traces of the nanoparticles were observed on few worn surfaces lubricated with S-CuO based lubricants. Only a few samples, not all, show the nanoparticles element on the worn balls. The main constituents of S-CuO nanoparticles i.e. Cu was observed in minute amount along with the majority of the ball material content. Probably, the S-CuO was harder as compared to ball material and continuous fatigue loading on these particles responsible for fracture of these particles. Under the higher contact stress, these fractured particles entrapped inside the worn surfaces and it can be identified in the EDS analysis.

5.3.2.2. Antifriction study

The variation in the COF throughout the test run has been presented in Figure 5.30. Average COF and interfacial shear stress values have enumerated in Table 5.8. It was observed that COF decreased continuously with the passing of time for nanoparticle based biolubricants, while it was almost constant with PO for lower concentrations range. The minimum average COF was observed for CO, RO, SO as compared with PO in lower concentration range. However, for higher concentration range (0.5%w/v or more) the impair friction property was observed. For raw oils, it was speculated that the improvement in the COF for bio-nanolubricants was due to the effectiveness of the oil polarity and chain length of hydrocarbon. On the other hand, for nanolubricant compositions the reduced real area of contact may be responsible. Papay (1983) reported that longer chain length of the base oil and stronger polarity of additive could form a thicker adsorb layer. Higher contact stress (≈ 3.4 GPa) developed during the test may cause thinning of the protective film but, it recovered itself by reorientation of base oil and additive molecules (Gupta and Harsha, 2017; Papay, 1983). Hence, variation in the COF was less and stable during the test. Hsu and Gates (2005)

also reported that, in boundary lubrication, reaction product and unreacted molecules between the contacting surfaces generate an ordered structure in the contact zone. Since these ordered structure has weakly bonded, thus results in low shear strength film between mating surfaces. It reflects low shear stress at the interface, which helps in improving antifriction performance. Also, the antiwear and antifriction behaviour of nanolubricant is a function of the real contact area (Ghaednia and Jackson, 2013). Hence, both of these phenomena attributed to the reductions in COF. In case of CO, RO and SO compositions, 0.1CCu (0.051), 0.1RCu (0.02) and 0.1SCu (0.0296) have shown minimum COF than other compositions (Table 5.8), thus considered as optimum. Also, this indicates lowest shear strength at optimum concentrations. It is speculated that 0.1%w/v amount of S-CuO was sufficient to provide threshold number of particles between the friction surfaces for asperity-asperity separation. It reduces the actual contact area and hence the minimum COF was observed. Beyond the concentration of 0.1%w/v, nanoparticles start to deteriorate the adsorbed tribo-film by the abrasion action.

On the contrary in case of PO compositions, the minimum COF observed for 1.0 PCu (i.e. 0.067), thus optimum. The first reason may be inability of asperity separation by formed tribo-film at lower concentrations. Second, at the lower concentrations the sufficient nanoparticles were not available to form a protective film on the mating surfaces due to the higher cohesive force among the nanoparticles. The maximum reductions in the average COF at optimum concentrations were 34.6, 70, 52.8 and 17.3% for CO, RO, SO and PO compositions, respectively.

Figure 5.31 represents the interfacial shear stress variation for all compositions. It shows the minimum interfacial stress at optimum concentrations. Also, shows similar trend as the

friction variation with the nanoparticles concentrations. Minimum interfacial stress exhibits significant reduction in COF.

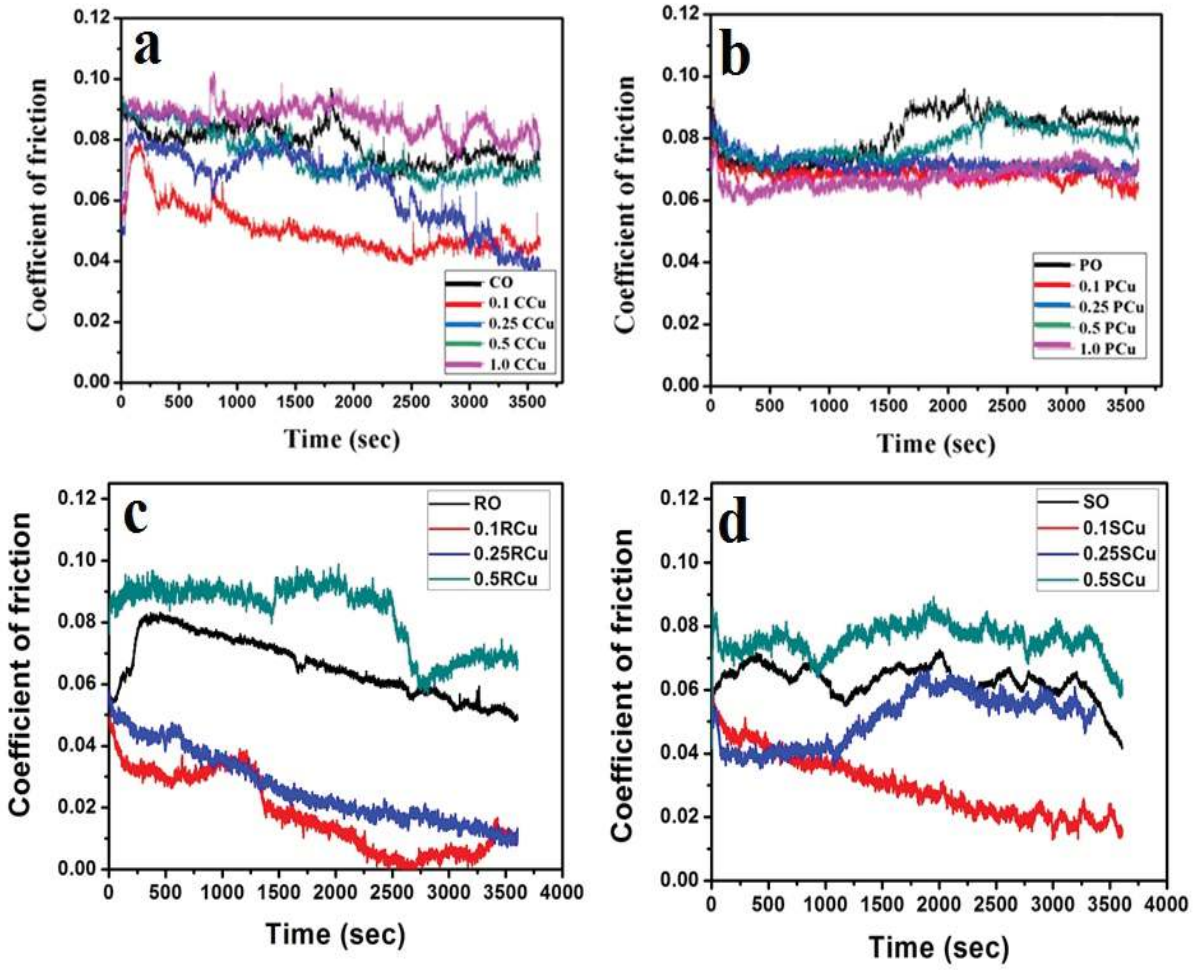

Figure 5.30. Variation in COF for different compositions of (a) CO, (b)PO, (c) RO and (d) SO; tested at load 392N, speed 1200 rpm for 1h.

Table 5.8. Average COF and interfacial shear stresses for different concentration of S-CuO with PO, CO, RO and SO. (σ: standard deviation for COF)

Oil compositions	Avg. COF	σ	Interfacial stress (MPa)
PO composition			
PO	0.081	0.0051	164.7
0.1PCu	0.068	0.0042	138.3
0.25PCu	0.072	0.0021	146.4
0.5PCu	0.078	0,0044	158.6
1.0PCu	0.067	0.0032	136.3
CO composition			
CO	0.078	0.0037	158.5
0.1CCu	0.051	0.0014	103.7
0.25CCu	0.064	0.0023	130.1
0.5CCu	0.074	0.0039	150.5
1.0CCu	0.086	0.0021	174.9
RO composition			
RO	0.0668	0.0006	135.8
0.1RCu	0.02	0.0013	40
0.25RCu	0.026	0.0036	52.8
0.5RCu	0.082	0.0062	166.8
SO composition			
SO	0.0628	0.0022	127.7
0.1SCu	0.0296	0.0038	60.2
0.25SCu	0.0506	0.0015	102.9
0.5SCu	0.0759	0.0022	154.4

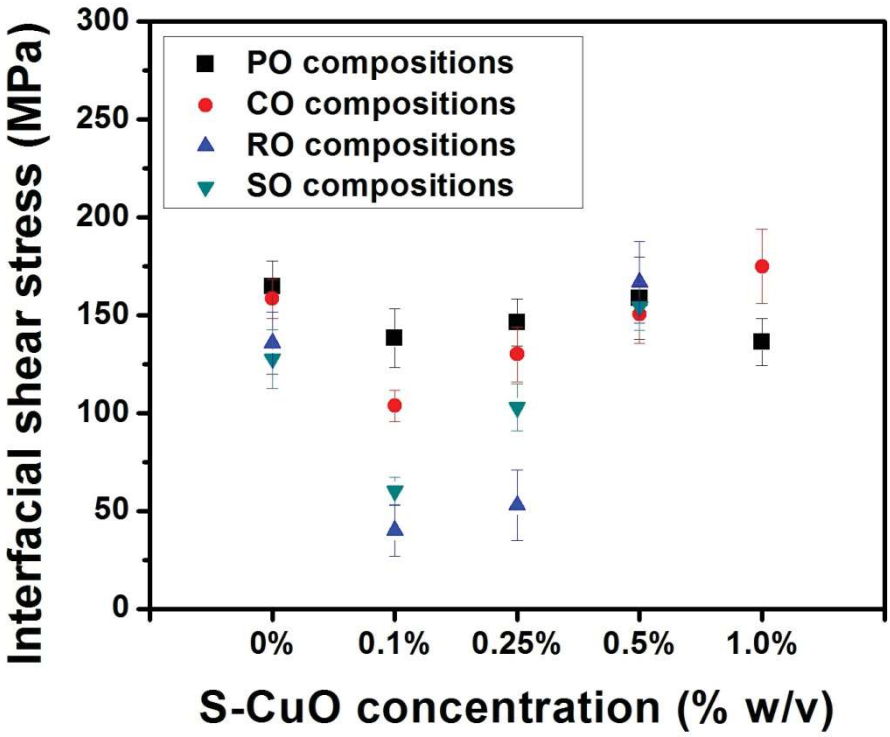

Figure 5.31. Variation in interfacial shear stress for different S-CuO base nanolubricant compositions. (Interfacial shear stress (τ) = COF x flow stress of the material)

5.3.2.3. Extreme-pressure study

The summary of the EP properties for all oil compositions presented in Table 5.9. The compositions for lower S-CuO concentration range (0.1 and 0.25%w/v) in base oils revealed the same last non-seizure and weld load as the base oils, which were 126 and 160 kgf respectively. However, EP properties improved substantially for higher concentration ranges (0.5 and 1.0%w/v). The maximum pass load was 160 kgf while weld load as 200 kgf. It elucidates that threshold number of nanoparticles might reach the mating surfaces and form a self protective layer which acts as nano-bearing. Also in the sliding contact, the localized heating was able to provide activation energy at the reaction site to produce a

pathway including hard, durable, and easily shearable components that helped in the load carrying ability of the oils (Hsu and Gates, 2005).

Table 5.9. Summary of EP performance for different S-CuO based nanolubricant compositions.

Oil compositions	Last non-seizure load (kgf)	Weld load (kgf)
PO composition		
PO	126	160
0.1PCu	126	160
0.25PCu	126	160
0.5PCu	126	160
1.0PCu	160	200
CO composition		
CO	126	160
0.1CCu	126	160
0.25CCu	126	160
0.5CCu	126	160
1.0CCu	160	200
RO composition		
RO	126	160
0.1RCu	126	160
0.25RCu	126	160
0.5RCu	160	200
SO composition		
SO	126	160
0.1SCu	126	160
0.25SCu	126	160
0.5SCu	160	200

5.3.3. Evaluation of tribo-performance for CeO_2 based lubricants

5.3.3.1. Antiwear study

Table 5.10 summarizes the WSD, MWV, wear reduction, and specific wear rate for all compositions of CeO_2 based nanolubricants. And, Figure 5.32 shows comparative study of WSD variation with distinct CeO_2 nano-additives concentration. It reveals that lower concentration range (0.1 or 0.25%w/v) improved the antiwear performance significantly. However, higher concentration range (0.5 or 1.0%w/v) starts to worsen the antiwear performance. For PO and CO compositions 0.25%w/v, while RO and SO composition exhibits 0.1%w/v of CeO_2 nano-additive as optimum due to lower WSD and highest wear reduction (Table 5.10). The negative sign in the wear reduction column as Table 5.10 represents WSD higher than the surfaces lubricated with base oils. This is the clear indication that CeO_2 nanoparticles from that particular concentrations start to abrade the interface. The highest reduction in WSD for PO, CO, RO and SO was 26.12, 33.93, 16.72 and 21% respectively. It can be seen that CO has shown higher concentration sensitive behavior with CeO_2 nanoparticles among other lubricants.

Figure 5.33 represents the SEM morphology of the worn surfaces tested with 0.25PCe composition of paraffin oil. It is an optimum composition. Lower magnification (Figure 5.33a) used to measure the WSD, while higher magnification reveals the worn surface topography (Figure 5.33b). At this concentration, shallow furrows were observed than the base oil. The topography of the worn surfaces at the optimum concentration of CeO_2 nanoparticles with all biolubricants presented in Figure 5.34. In all the cases mild trenches and scratches were revealed. A small material transfer was observed in few cases, which

indicates the adhesive wear phenomenon is also responsible for material wear. Figure 5.35 represents the specific wear rate of nanolubricants at different concentrations. The optimum concentration of CeO_2 nanoparticles reveals the minimum specific wear rate (Table 5.10). The variation in MWV and specific wear rate has also shown similar behavior as WSD variation. In other words, calculated MWV and specific wear rate exhibits the lowest magnitude as compared to the other compositions. This is because of direct proportional relation with the WSD.

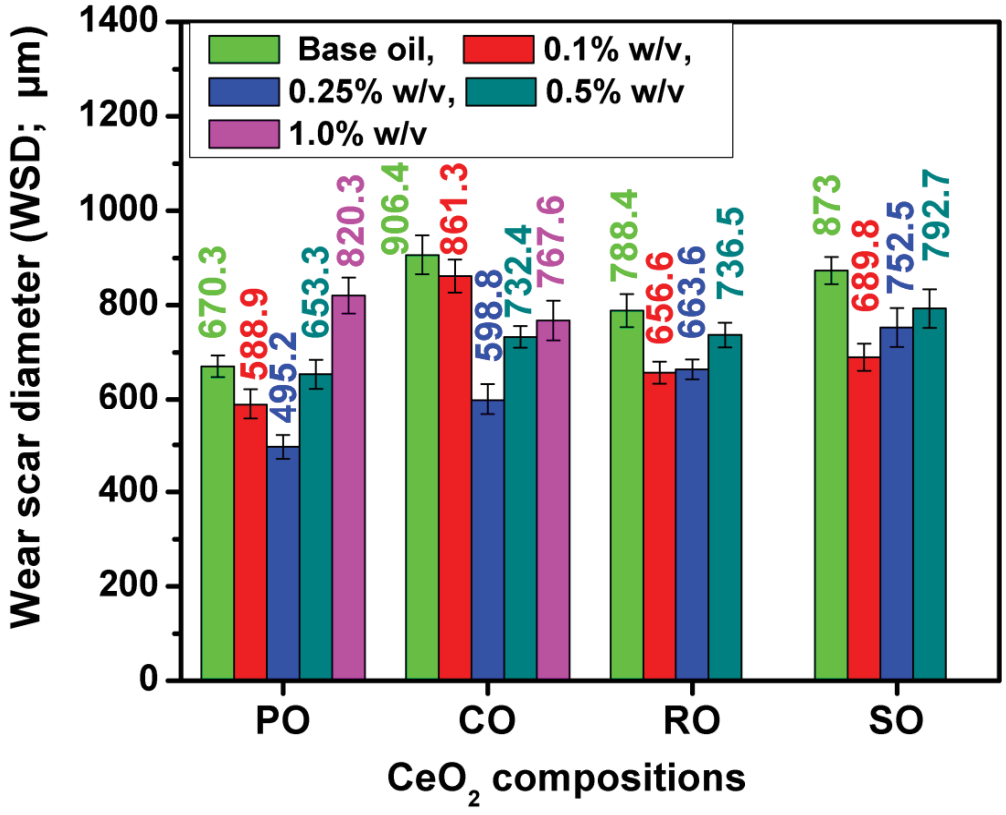

Figure 5.32. Comparative variation in WSD for all CeO_2 based nanolubricant compositions tested with 392N load, 1200 rpm speed for 1h.

Table 5.10. Summary of WSD, wear reduction (WR), mean wear volume (MWV) and specific wear rate for different concentration of CeO_2 with PO, CO, RO and SO.

Oil compositions	WSD (µm)	WR (%)	MWV ($x10^{-4}$ mm^3)	Specific wear rate (m^3/N-m)
PO composition				
PO	670.3	…	28.42	1.07×10^{-17}
0.1PCe	588.9	12.14	16.14	0.608×10^{-17}
0.25PCe	495.2	26.12	7.23	0.278×10^{-17}
0.5PCe	653.3	2.54	25.44	0.96×10^{-17}
1.0PCe	820.3	-22.4	66.58	2.51×10^{-17}
CO composition				
CO	906.4	…	100.5	3.79×10^{-17}
0.1CCe	861.3	4.97	81.5	3.07×10^{-17}
0.25CCe	598.8	33.93	17.4	0.655×10^{-17}
0.5CCe	732.4	19.2	41.4	1.56×10^{-17}
1.0CCe	767.6	15.3	50.5	1.9×10^{-17}
RO composition				
RO	788.4	…	56.4	2.13×10^{-17}
0.1RCe	656.6	16.72	26.0	0.98×10^{-17}
0.25RCe	663.6	15.83	27.2	1.026×10^{-17}
0.5RCe	736.5	6.58	42.4	1.599×10^{-17}
SO composition				
SO	873.0	…	86.1	3.25×10^{-17}
0.1SCe	689.8	21.0	32.1	1.21×10^{-17}
0.25SCe	752.5	13.8	46.4	1.75×10^{-17}
0.5SCe	792.7	9.2	57.7	2.18×10^{-17}
Negative sign indicates impaired antiwear property.				

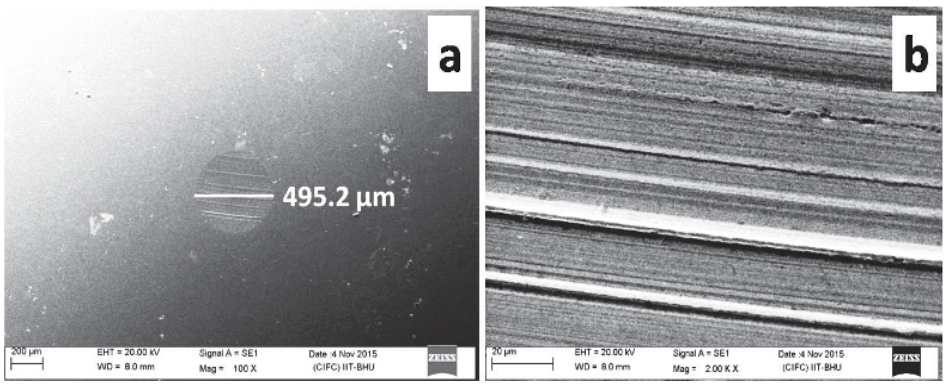

Figure 5.33. SEM image of 0.25PCe composition of paraffin oil at different magnifications [load 392N, sliding speed 1200 rpm, time 1h].

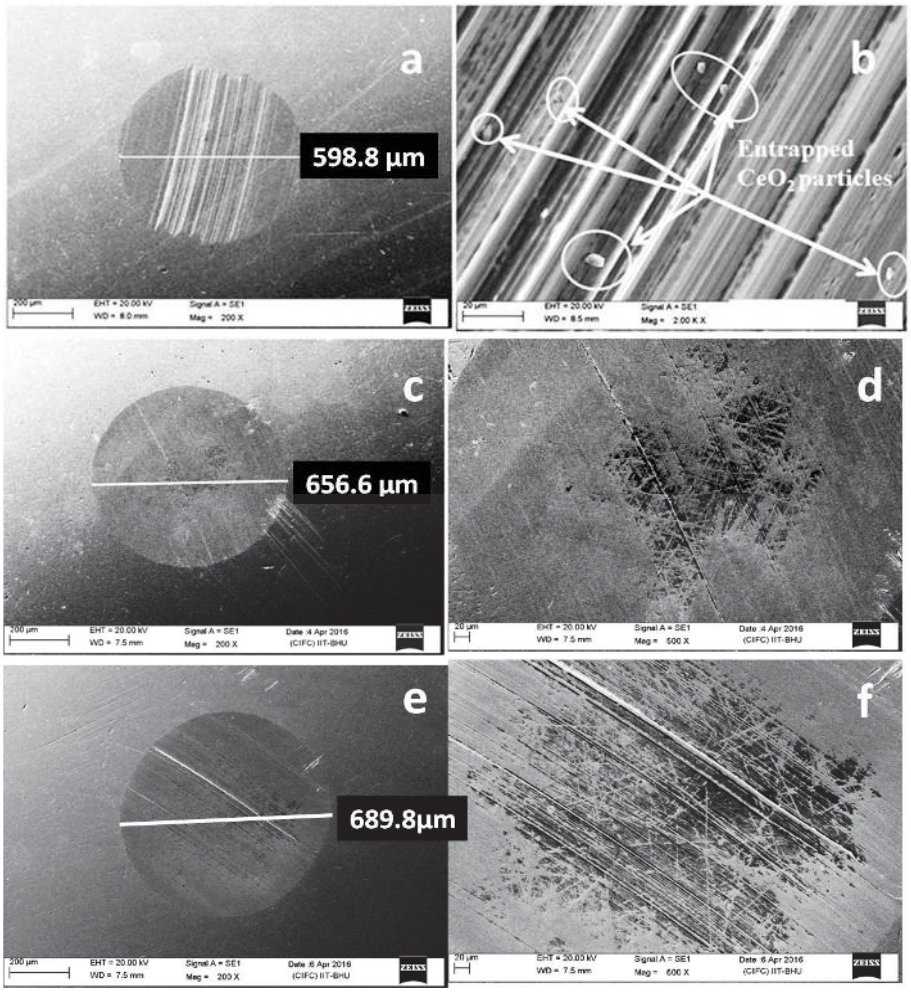

Figure 5.34. SEM image of worn surfaces for optimum compositions of bio-nanolubricants (a, b) 0.25CCe ; (c,d) 0.1RCe ; and (e, f) 0.1SCe at different magnifications. [load 392N, sliding speed 1200 rpm, time 1h]

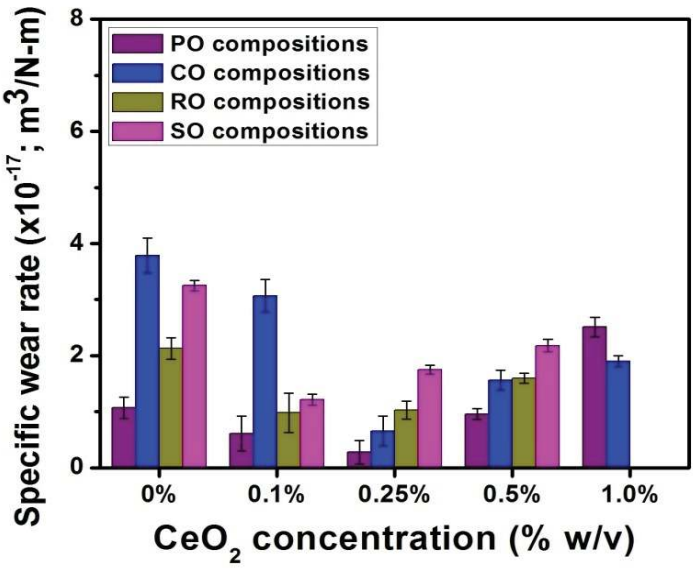

Figure 5.35. Comparative variation in specific wear rate for all compositions of CeO_2 based nanolubricants.

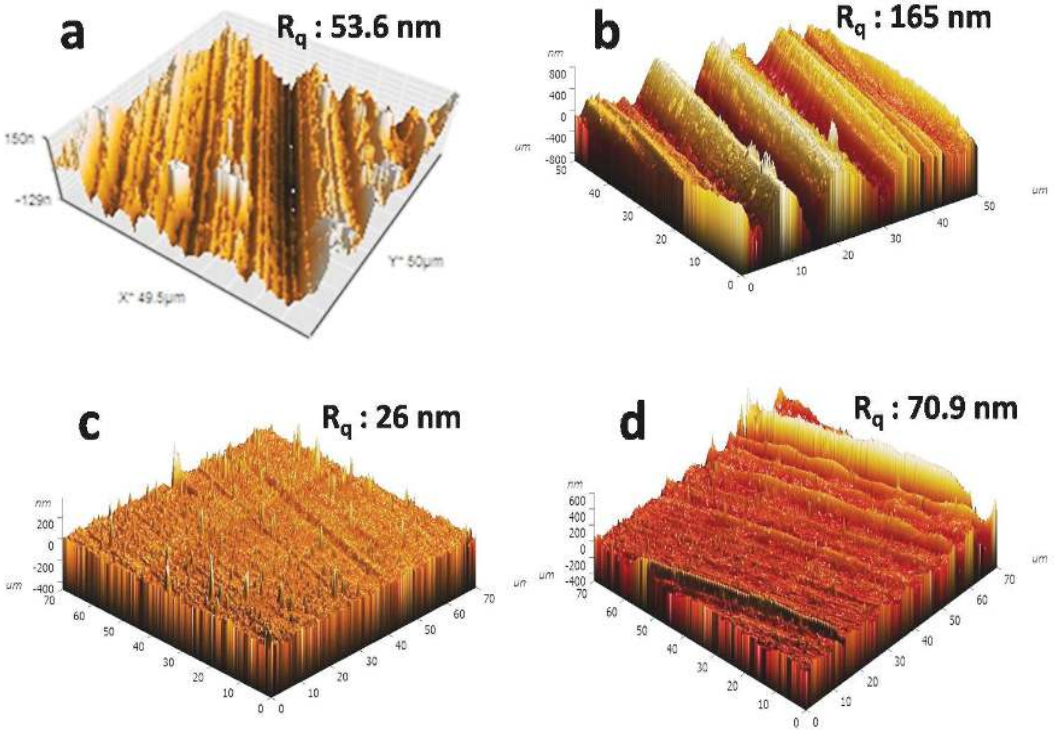

Figure 5.36. AFM roughness images of worn track tested with 392N load, speed 1200 rpm, for 1h at optimum concentration (a) 0.25PCe ; (b) 0.25CCe ; (c)0.1RCe and (d) 0.1SCe.

Figure 5.36 depicts the worn surface roughness images for all CeO_2 based oil compositions at optimum concentrations (as WSD variation). The roughness values measured in the cross direction of the worn track. For PO, CO, RO and SO compositions, the line roughness (R_q) were 53.6, 165, 46, and 70.9 respectively, while surface roughness (S_q) was 62.7, 149.2, 61 and 83.6 nm respectively. As compared to the base oils without any additive a substantial reduction in the roughness was observed for nanolubricants. Especially at the optimum concentration, it exhibits comparative smoother surface thus the lowest roughness value.

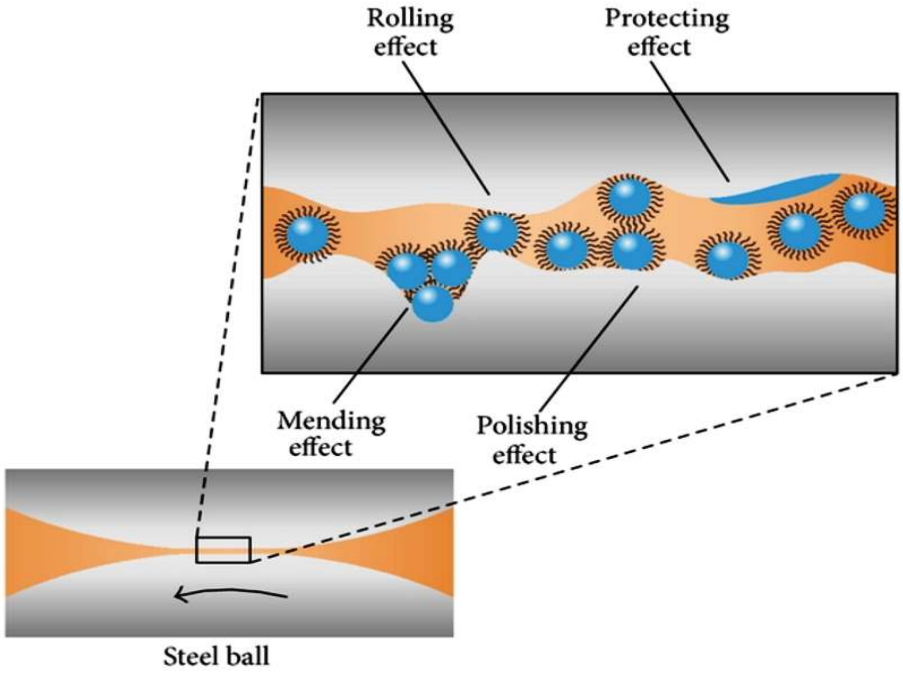

Figure 5.37. Typical image of nanoparticle based lubricant interaction at mating surfaces showing mending, polishing, rolling effect. (Sui et al., 2015)

The hypothetical image of a possible reason for the improvement is depicted in Figure 5.37. The variations in the size of the nanoparticles have a major role in obtaining the mending, rolling effect and morphology reflects the polishing mechanism. As the average size of 100

CeO_2 particles was 80 nm with variation from 34.2 to 121 nm. The smaller particles fill the valleys and dimples to smoothen the interface, and bigger one takes the fractional load. Irregular shape polishes the surface by minute removal of material to smooth the surface. The rolling behavior of the nanoparticles between the mating surfaces (to act as nano-bearing as discussed in section 5.3.1.1) also responsible for such improvement in antiwear properties. The tribosinterisation mechanism may also play a critical role under the operating sliding condition. In tribosinterisation, nano-additive containing valleys get compacted by the asperities under higher pressure and localized temperature. It forms a compact protective film and prevent/reduce metal to metal contact thus incisive tribological properties. This mechanism is applicable only when the particle size is very small so that it can enter in the surface valleys or dimples easily. These cases are viable up to the specific concentration, as in our case lower concentration ranges (0.1 or 0.25%w/v). At a higher concentration range (0.5%w/v or more) the inter-particle distance becomes less and cohesive force dominates. It degrades suspension property of nanoparticles due to agglomeration, thus effect on the tribological property. Appendix-C shows the suspension abilities of different nanoparticles in the lubricants.

5.3.3.2. Antifriction study

The magnitudes of the mean COFs presented in Table 5.11. It shows the antifriction behavior of the nanoparticle based lubricant either PO or biolubricants improved as compared to the base oils. The lower concentration range exhibits better antiwear property as compared to higher concentration range. The maximum reduction in mean friction coefficient for PO, CO, RO and SO compositions were 29.6, 43.3, 74.5 and 22.3% respectively. CO and RO show superior antiwear behavior as compared to the PO. The reason for such action attributed to

the existence of the functional group (like hydroxyl) in the fatty acid structure and the rapid formation of the protective film which separates the mating surfaces.

Table 5.11.Average COF and interfacial shear stresses for different concentration of CeO_2 with PO, CO, RO and SO. (σ: standard deviation for COF)

Oil compositions	COF (Avg.)	σ	Interfacial stress (MPa)
PO composition			
PO	0.081	0.0051	164.7
0.1PCe	0.066	0.0046	134.2
0.25PCe	0.057	0.0024	115.9
0.5PCe	0.071	0.0029	144.4
1.0PCe	0.086	0.0040	174.9
CO composition			
CO	0.078	0.0037	158.5
0.1CCe	0.0537	0.0043	109.2
0.25CCe	0.0442	0.0019	89.9
0.5CCe	0.0574	0.0034	116.7
1.0CCe	0.0585	0.0028	118.9
RO composition			
RO	0.0668	0.006	135.8
0.1RCe	0.017	0.0017	34.6
0.25RCe	0.046	0.0039	93.5
0.5RCe	0.052	0.0041	105.7
SO composition			
SO	0.0628	0.0022	127.7
0.1SCe	0.0488	0.0023	99.2
0.25SCe	0.0574	0.0052	116.7
0.5SCe	0.0713	0.0066	145.0

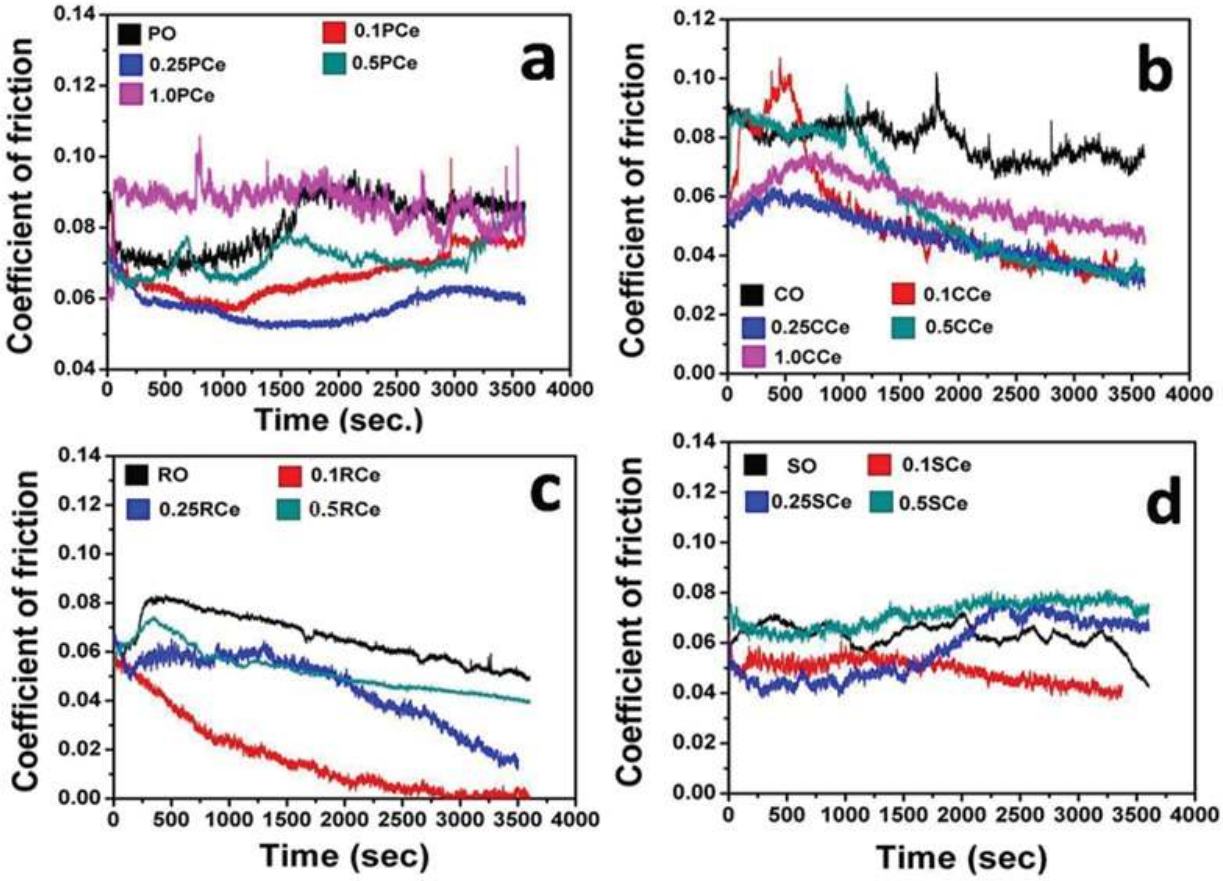

Figure 5.38. Variation in friction coefficient for all concentration of CeO_2 in (a) PO; (b) CO; (c) RO and (d) SO; at load 392N, sliding speed 1200 rpm, time 1h.

The variation of COF during the test run presented in the Figure 5.38 for all compositions of PO and biolubricants. For PO compositions (Figure 5.38a), it observed that up to 1500 seconds the friction decreases and then increased continuously. This phenomenon was observed up to 0.5%w/v concentration of the CeO_2 nanoparticles. Above this concentration, friction trend is almost constant and higher than the base PO itself. It indicates lump formation of the nanoparticles at a higher concentration which abrades the interface. Figure 5.39 shows the shear stress variation at the interface for different nanolubricant compositions. It exhibits that at 0.25%w/v amount of CeO_2 shows minimum stress with PO. Minimum

interfacial stress results in lower COF because of direct proportionality. As compared to the biolubricant compositions PO compositions show comparative higher interfacial stress.

For CO compositions (Figure 5.38b), the continuous decrement in the friction behavior was observed for nanolubricants throughout the test. During initial few seconds, increase in the COF indicates a wear-in period. As compared to the base CO, the friction behavior shows improvement with nanolubricants for all CO compositions. Interfacial shear stress shows good agreement with the mean COF trend. Similar observation also observed for the RO compositions (Figure 5.38c). However, for SO compositions, nanolubricants show the almost constant behavior throughout the test run similar to the paraffin oil, except 0.1%w/v concentration. This behavior can be correlated with the oil viscosity. In other words, CO and RO the viscosity was higher as compared to the SO and PO. Thus nanoparticle suspension was better and it is reflected in tribo-performance.

Figure 5.40 represents the typical role of surface and sub-surface of the substrate on friction behaviour. The uppermost layer of the substrate, known as Beilby layer, often has crystalline and amorphous in nature (Sahoo et al. 2011). Therefore, under higher loading conditions this layer distorted firstly and form secondary ultrafine particles. Thereafter, the oil molecules reaches to other sub-surfaces i.e. compound oxide and deformed layer by traversing through top layer. And, here it forms a strongly bonded adsorbed film that has potential to separate the asperities. In the lower nano-additive concentration range, the generated secondary ultrafine particles also help in mending and tribositerisation. Also, these particles support in rolling-sliding action and keeps mating surface away. Probably, it helps to obtain improved friction performance during sliding. However with higher concentration range (i.e. 0.5 or 1.0%w/v in our case), nano-additives tend to aggregate due to high intermolecular attraction.

Therefore, these clustered particles abrade the compound oxide and deformed layer, thus impaired friction property.

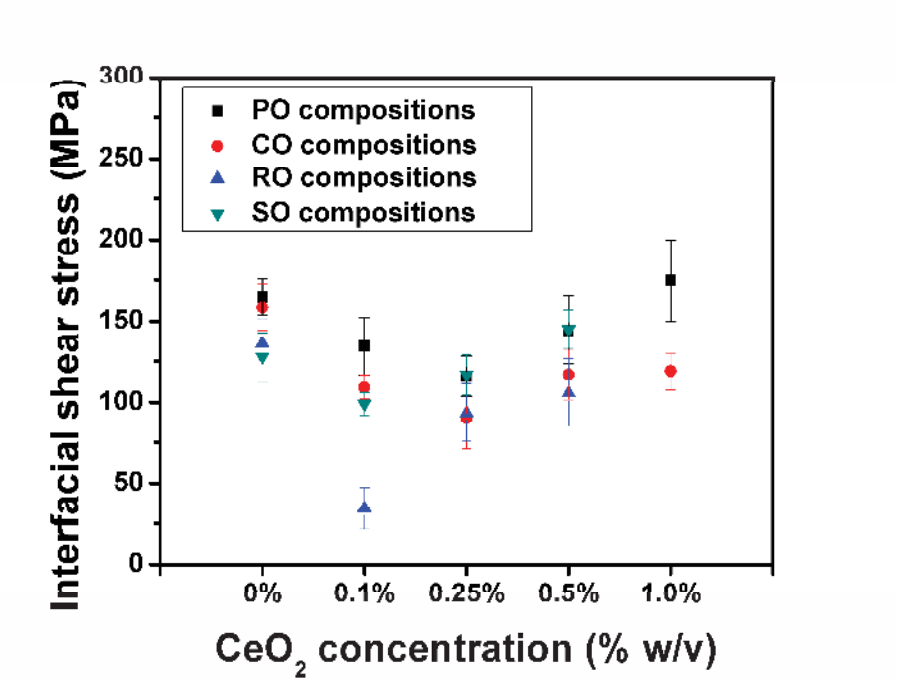

Figure 5.39. Variation in interfacial shear stress for all CeO_2 based nanolubricant compositions.

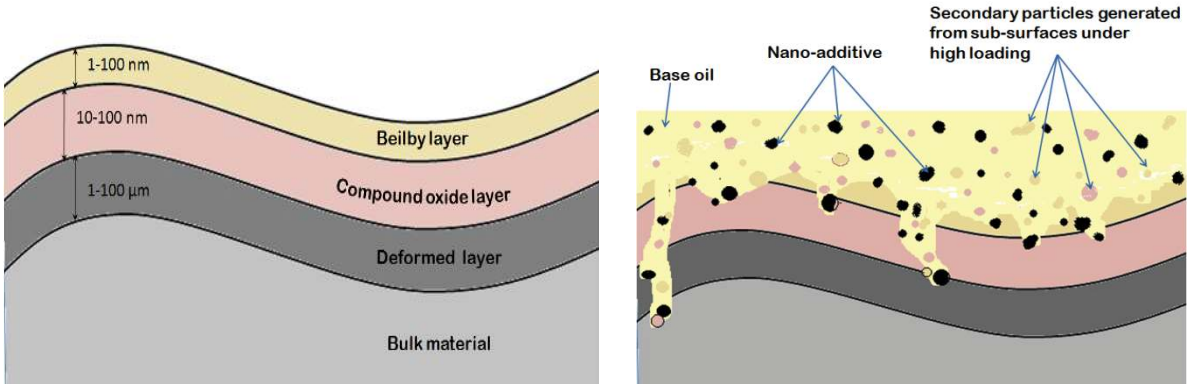

Figure 5.40. Proposed hypothetical mechanism of nanolubricant in contact zone to influence the tribological behavior.

5.3.3.3. Extreme-pressure study

The EP properties of the CeO_2 based nanolubricants summarized in Table 5.12. The base oils show 126 and 160 kgf as the pass and weld load, respectively. Therefore, load carrying capacity of the lubricant marked as 126 kgf.

Table 5.12. Summary of EP behavior for all CeO_2 based nanolubricant compositions.

Oil compositions	**Last non-seizure load (kgf)**	**Weld load (kgf)**
PO composition		
PO	126	160
0.1PCe	126	160
0.25PCe	126	160
0.5PCe	126	160
1.0PCe	160	200
CO composition		
CO	126	160
0.1CCe	126	160
0.25CCe	126	160
0.5CCe	160	200
1.0CCe	160	200
RO composition		
RO	126	160
0.1RCe	126	160
0.25RCe	126	160
0.5RCe	160	200
SO composition		
SO	126	160
0.1SCe	126	160
0.25SCe	126	160
0.5SCe	160	200

For all nanolubricant compositions, lower concentration range (up to 0.25%w/v in this study) showed the similar EP property as that of base oils. However, 0.5%w/v or more amount showed a substantial improvement in load carrying capacity from 126 to 160 kgf (Table 5.12). Therefore for PO compositions 1.0%w/v and for all nanoparticles based biolubricants 0.5%w/v is considered as optimum concentrations.

In this case, also the lower concentrations of CeO_2 nanoparticles do not show any positive/ adverse effect on the base oil property. However, lubricants with a higher concentration of nanoparticles in the PO have improved its EP property significantly. The reason for such behaviour may include squeezing out of the nanoparticles at the interface due to high load and rotational speed. Also, at higher concentration, the nanoparticles can stay at the interface even at high load and speed. It separates the asperity-asperity collision and avoids welding of the balls. Srinivas et al. (2017) have also observed the similar variations in the weld load with change in concentrations of molybdenum disulfide nanoparticles in SAE 20W-40 grade oil, and they reported that the weld load capacity of nanolubricant improved at 0.5 wt% concentration of molybdenum disulfide as an additive.

5.3.4. Evaluation of tribo-performance for PTFE based lubricants

5.3.4.1. Antiwear study

Antiwear results for the PTFE based nanolubricant compositions presented in Table 5.13 and Figure 5.41. It is clear that for all PO compositions with PTFE, no improvement in WSD observed at any concentration. The WSD increased with the addition of the PTFE nanoparticles. However, PTFE with CO, RO and SO has shown substantial improvement in WSD. Maximum reductions of 48.75% and 31.46% were observed for 0.1RP and 0.1CP

respectively. Although, 0.5SP also reduced the WSD it was very low as compared with CO and RO optimum compositions. However, other concentrations also reduced the wear substantially (Table 5.13). Xie et al. (2016) and Peng et al. (2009) have also reported the optimality conditions for tribo-performance with paraffin oil blended with diamond and SiO_2.

For PTFE based nanolubricants, there are three parameters viz. elastic property of PTFE, viscosity and fatty acid structure of biolubricants have vital role to reflect the antiwear behavior. Elastic property provides the cushioning effect at the interface. And, the higher viscous lubricant may suspend the nanoparticles for a longer time as compared to low viscous oil as CO and RO in our case. Also, fatty acid structure, oil polarity and variation in the size of nanoparticles have important role in achieving the enhanced tribo-performances. It is speculated that combination of the oleic acid and linoleic acid content in fatty acid chain reflects the tribo-performance. One can say that the formation rate and thickness of the protective tribo-film is dependent on oleic acid and linoleic acid content. Reeves and Menezes (2017) studied the influence of fatty acid compositions on tribological performance with different biolubricants. They reported that oleic acid have tendency to form thicker monolayer film on the contact zone to protect counter surfaces. Since the density of PTFE is quite low therefore good suspension in the lubricant (Sang, 2015). Thus during sliding it participated to form quick and thick protective layer on mating surfaces. PTFE also exhibits good concentration sensitive behavior with all the biolubricants. This is because of substantial change in WSD with slight variation in the concentration.

Since SDS was used in this study as dispersing agent and it contains polar head and non-polar tail group. Figure 5.42 shows the typical interaction among oil molecules, SDS and nanoparticles. Here head group attached with oil molecules while tail group with

nanoparticles surface. It provides longer suspension of additive, which is essential for obtaining incisive tribo-performance. Also, Yan et al. (2014) reported about the similarity rule that similar polarity between additive and oil molecules provides better affinity, thus reflects tribological behavior.

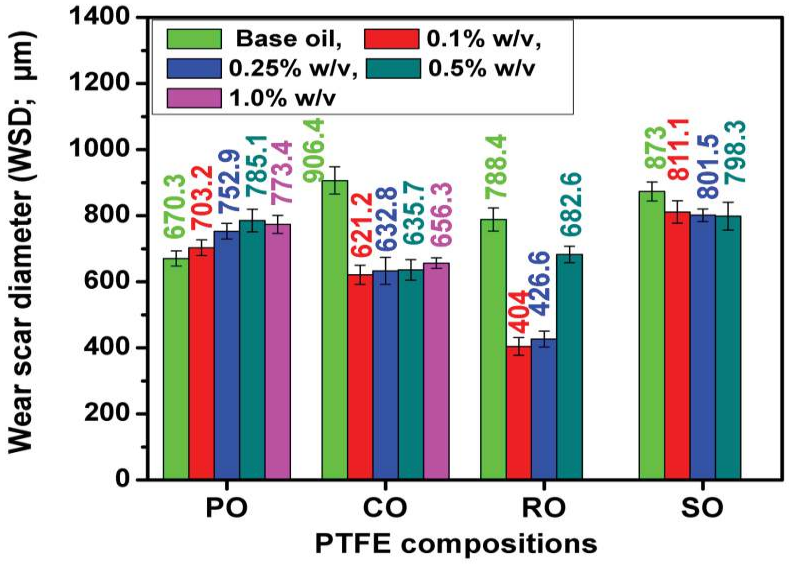

Figure 5.41. Comparative WSD variation for all PTFE based nanolubricant compositions tested at 392N load, 1200 rpm speed for 1h.

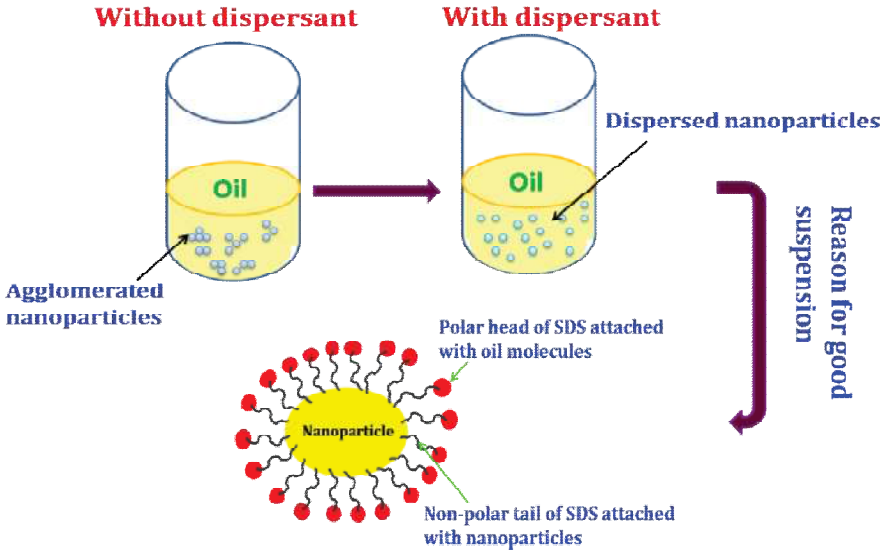

Figure 5.42. Schematic diagram showing the effect of SDS dispersant on the suspension of nanoparticles in lubricant.

Figure 5.43 and 5.44 depict the SEM topography of the worn-out surfaces at the optimum PTFE concentrations with CO, RO and SO respectively. Overall smoother surfaces observed with the optimum PTFE concentrations with all the biolubricants. In few of the samples, clear evidence of the protective layer was revealed in SEM images as Figure 5.43b. Also, the elements of the additive with the majority of iron were identified in the elemental analysis with EDS as shown in Figure 5.45. Probably, PTFE under higher contact stress and sliding speed can slip like the lamellar structure. Under localized frictional heating PTFE get activation energy and produces denser protective layer on the contacting surfaces. In another observation for PTFE and SO compositions, it can assume that at the lower amount (0.1 or 0.25%w/v) the mating surfaces are not separated sufficiently. Thus, somewhere adhesive wear was predominant along with abrasion (Figure 5.44a-d).

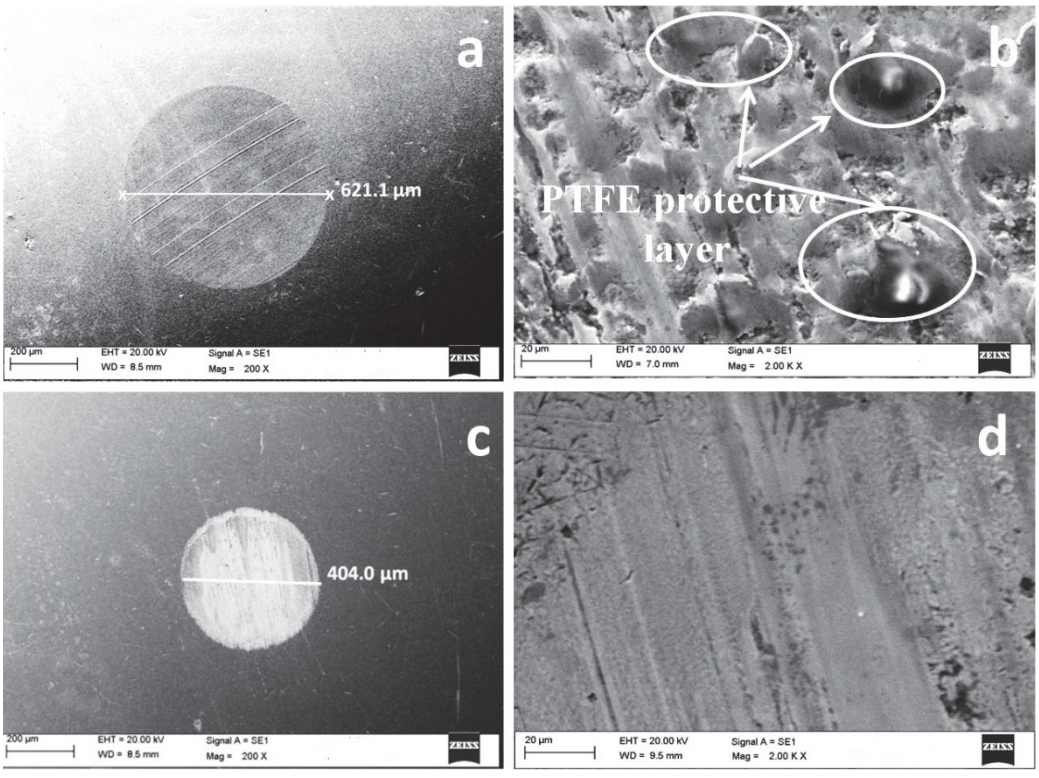

Figure 5.43. SEM morphology of worn surfaces tested with (a, b) 0.1CP and (c, d) 0.1RP at different magnification (optimum concentration). (Load 392N, speed 1200 rpm, time 1h)

Table 5.13. WSD, wear reduction (WR), mean wear volume (MWV) and specific wear rate for different concentration of PTFE with PO, CO, RO and SO.

Oil compositions	WSD (µm)	WR (%)	MWV (x10^{-4} mm^3)	Specific wear rate (m^3/N-m)
PO composition				
PO	670.3	…	28.42	1.07×10^{-17}
0.1PP	703.2	-4.9	34.8	1.31×10^{-17}
0.25PP	752.9	-12.3	46.5	1.75×10^{-17}
0.5PP	785.2	-17.1	55.5	2.09×10^{-17}
1.0PP	773.4	-15.4	52.1	1.96×10^{-17}
CO composition				
CO	906.4	…	100.5	3.79×10^{-17}
0.1CP	621.2	31.46	20.4	0.77×10^{-17}
0.25CP	632.8	30.2	22.2	0.835×10^{-17}
0.5CP	635.7	29.86	22.6	0.852×10^{-17}
1.0CP	656.3	27.6	25.9	0.98×10^{-17}
RO composition				
RO	788.4	…	56.4	2.13×10^{-17}
0.1RP	404.0	48.75	2.4	0.092×10^{-17}
0.25RP	426.6	45.89	3.3	0.12×10^{-17}
0.5RP	682.6	13.4	30.7	1.16×10^{-17}
SO composition				
SO	873.0	…	86.1	3.25×10^{-17}
0.1SP	811.7	7.02	63.7	2.4×10^{-17}
0.25SP	801.5	8.19	60.4	2.28×10^{-17}
0.5SP	798.3	8.56	59.5	2.24×10^{-17}
Negative sign indicates impaired antiwear property.				

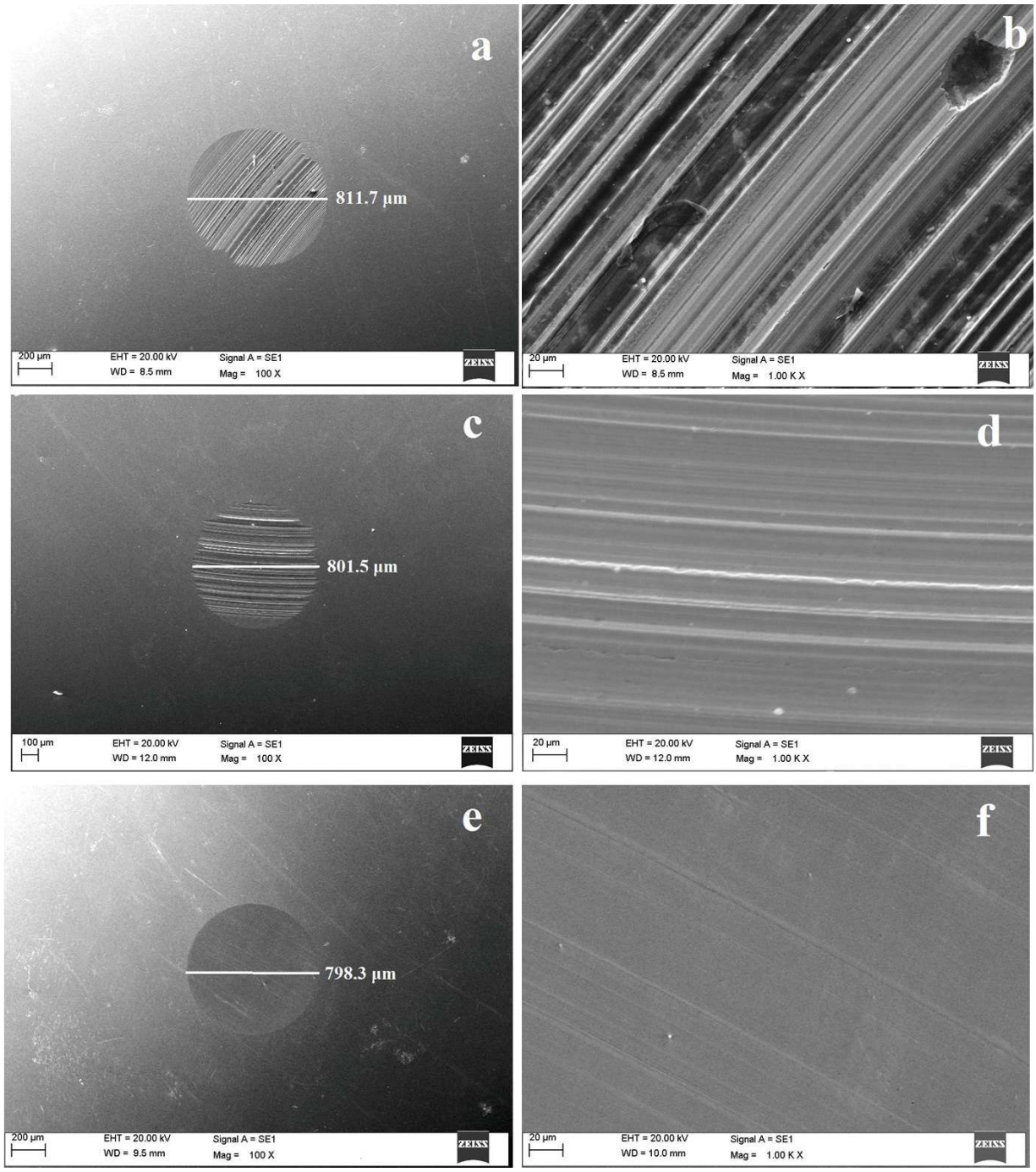

Figure 5.44. SEM morphology of worn surfaces tested with PTFE in SO at; (a, b) 0.1 , (c,d) 0.25 and (e, f) 0.5%w/v concentration. (load 392N, speed 1200 rpm, time 1h)

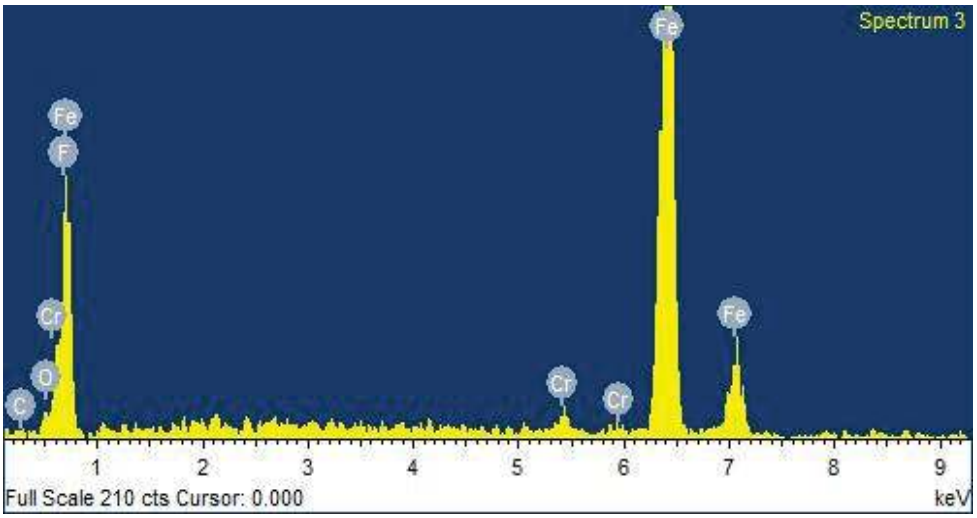

Figure 5.45. Typical image of the worn track lubricated with PTFE based nanolubricants.

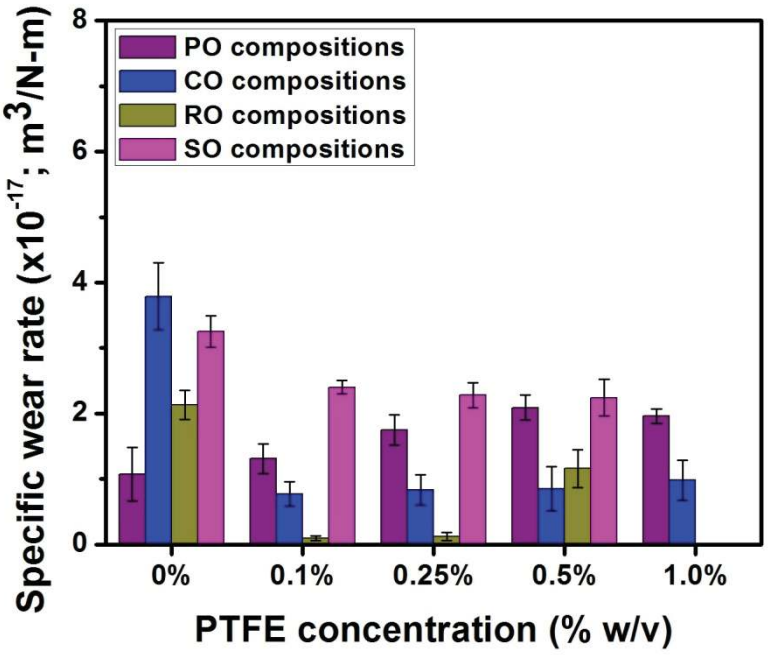

Figure 5.46. Variation in specific wear rate for all nanolubricant composition with PTFE.

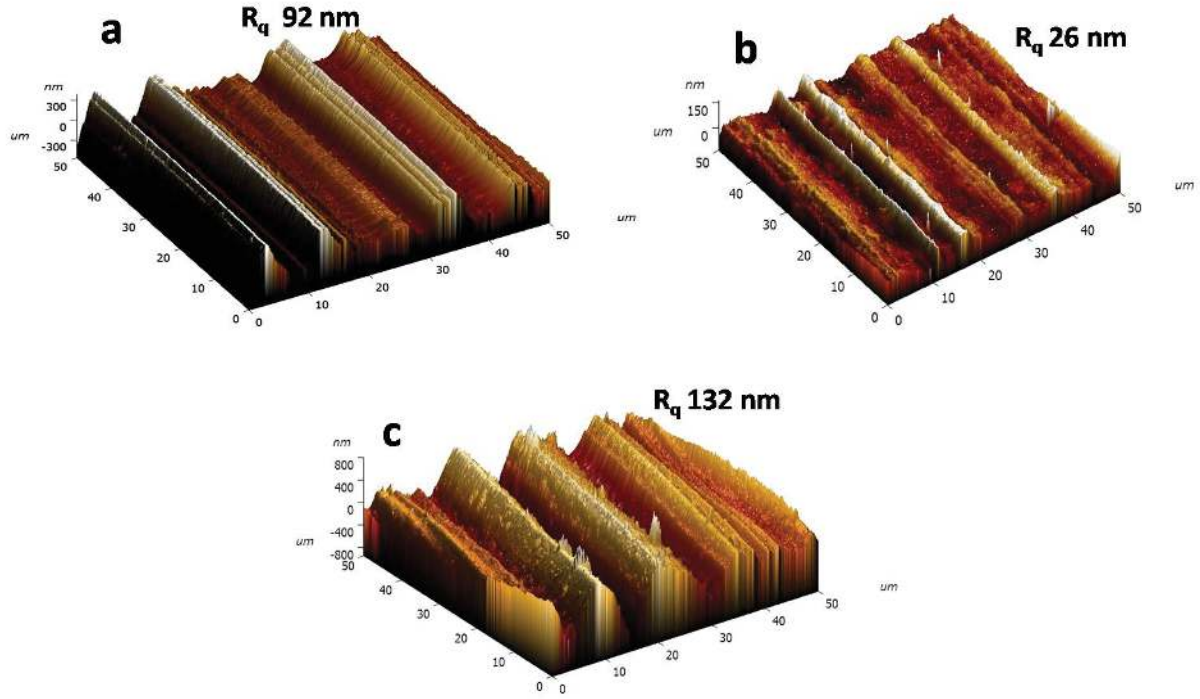

Figure 5.47. Roughness images of the worn surfaces (for optimum compositions) (a) 0.1CP (b) 0.1RP and (c) 0.5SP. (tested at 392N load, 1200 rpm speed for 1h)

The variation of specific wear rate (for all compositions) and AFM roughness images at optimum PTFE concentrations have been presented in Figure 5.46 and 5.47 respectively. The variation in specific wear rate shows the in-line variation with the WSD because of the direct proportionality. CO, RO and SO with respective optimum concentrations of PTFE reduced the roughness (R_q) by 76.9, 90.4 and 54.8% as compared to respective base oil lubrication.

5.3.4.2. Antifriction study

The summary of the antifriction behaviour presented in Table 5.14. The average COF for PTFE and PO composition was reduced slightly about 7.5% (at 0.25PP) as compared to the

PO. However, with CO, RO and SO it was reduced by 64.1, 62.5 and 27.5% (maximum) for optimum compositions.

Table 5.14. Mean COF and interfacial shear stresses for different concentration of PTFE with PO, CO, RO and SO. (σ: standard deviation for COF)

Oil compositions	COF (Avg.)	σ	Interfacial stress (MPa)
PO composition			
PO	0.081	0.0051	164.7
0.1PP	0.0796	0.0068	161.9
0.25PP	0.0749	0.0034	152.3
0.5PP	0.101	0.0044	205.4
1.0PP	0.095	0.0039	193.2
CO composition			
CO	0.078	0.0037	158.5
0.1CP	0.0447	0.0028	90.9
0.25CP	0.0358	0.002	72.8
0.5CP	0.0285	0.0018	57.9
1.0CP	0.0287	0.0021	58.4
RO composition			
RO	0.0668	0.0006	135.8
0.1RP	0.025	0.0005	50.8
0.25RP	0.027	0.0011	54.9
0.5RP	0.035	0.0009	71.2
SO composition			
SO	0.0628	0.0022	127.7
0.1SP	0.0915	0.0056	186.1
0.25SP	0.0772	0.0072	157.0
0.5SP	0.0455	0.0023	92.5

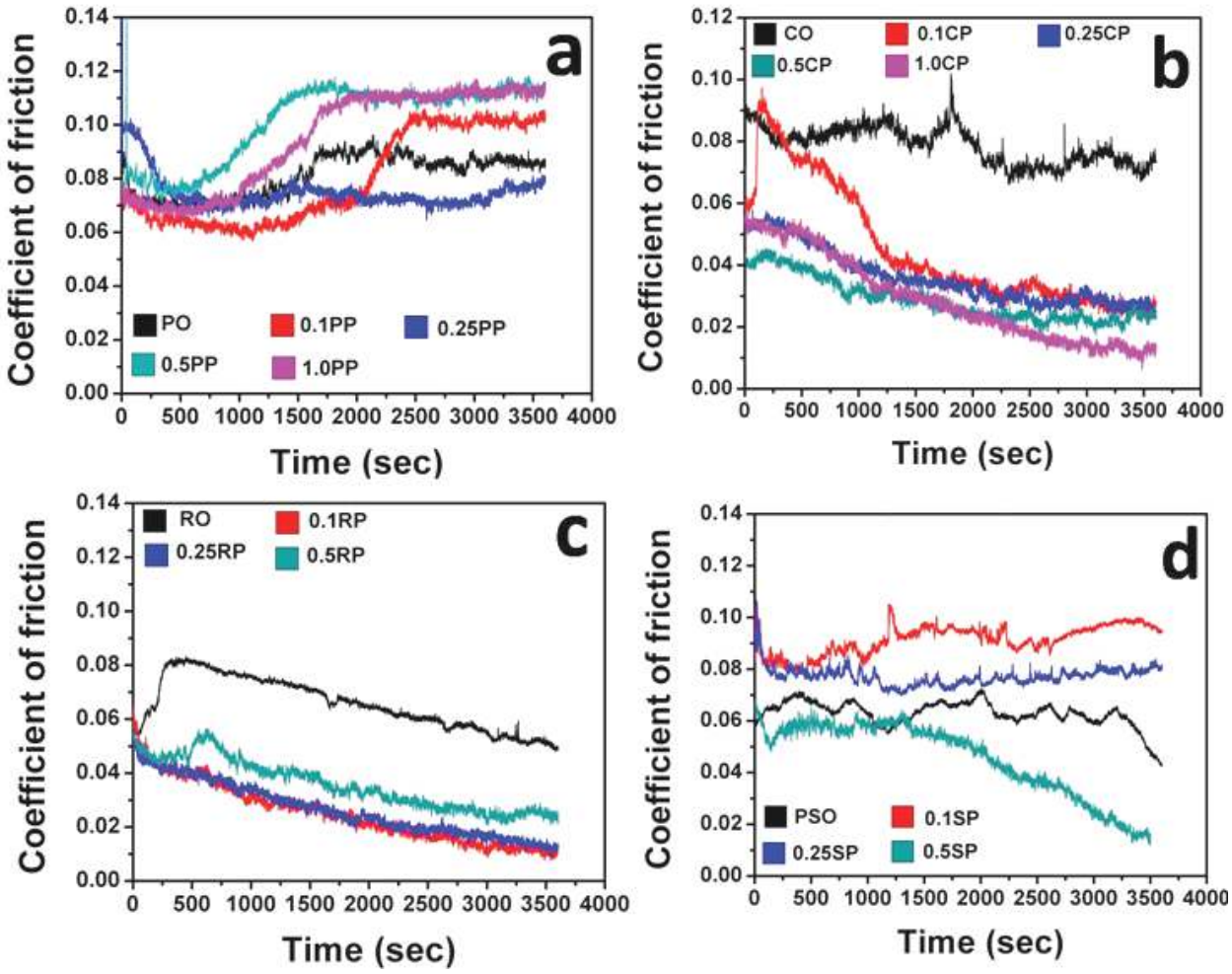

Figure 5.48. Variation in COF for all the PTFE concentration tested at 392N load for 1h with (a) PO, (b) CO, (c) RO and (d) SO.

Figure 5.48 depicts the variation of COF throughout the test run. For all PO compositions with PTFE (Figure 5.48a) including base PO, the behavior of friction curve is similar. For first few seconds the friction is slight decreasing/constant then increasing throughout the test run. It signifies that PTFE did not show compatible behavior with the PO at any concentration. The formed protective film on the mating surfaces could not retain its beneficial property for a longer time. Probably, the non-polar nature of the oil did not attract the PTFE nanoparticles too much towards the interface even after the use of the surfactant

SDS. On the contrary, PTFE with biolubricants (Figure 5.48b-d) has shown a significant reduction in friction curve up to the asymptotic value. With the close observation for different biolubricants with PTFE, it was found that CO and RO show a substantial reduction in friction at lower concentration range. However, SO indicates the improvement at higher concentration range. The viscosity of the biolubricants may have a key role in this regards. Because CO and RO have a higher viscosity as compared to SO, thus low density PTFE nanoparticles might be in the suspended state in the base oils for a longer time. The suspension images of various PTFE based nanolubricants are presented in Appendix-C. Also, diffusion of the PTFE occurs under localized heating and formation of mono- or multi layer film provides cushioning effect to the counter surfaces. Thus, improved friction performance observed.

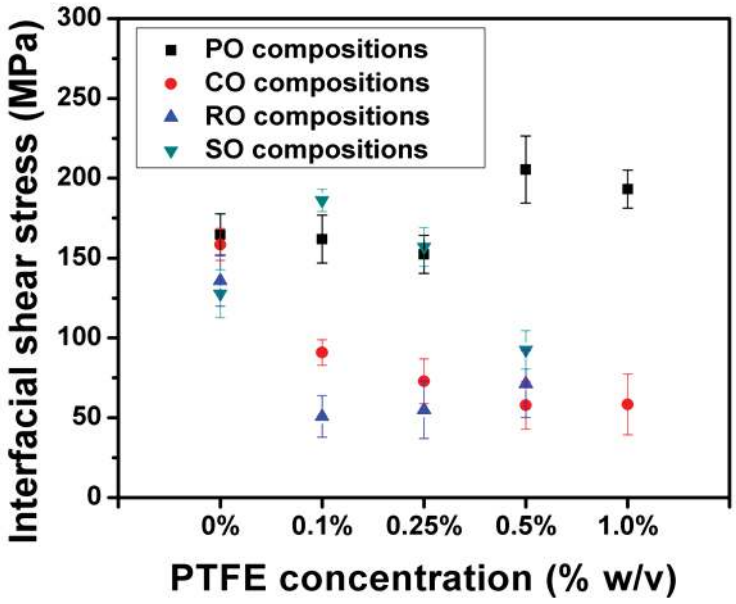

Figure 5.49. Interfacial shear stress for PTFE based nanolubricants.

The interfacial shear stress for all the concentrations with the base oils presented in Figure 5.49. The trend of the nanolubricants shows good agreement with the mean COF variation.

At all the PTFE compositions with PO, CO, RO and SO, the calculated minimum interfacial shear stresses were 152.3, 57.9, 50.8 and 92.5 MPa respectively (Table 5.14). Thus, the nanolubricants having lower interfacial stress exhibits better lubrication.

5.3.4.3. Extreme-pressure study

No improvement in the EP properties was observed at any concentration of PTFE with any base lubricants. At all the concentrations nanolubricants behave similarly to the base oils. In other words, for each PTFE composition the pass and weld loads were 126 and 160 kgf respectively. It is attributed to inability of PTFE nanoparticles to carry higher applied load under high sliding speed conditions.

5.4. Summary of the chapter

The biolubricants show higher concentration sensitive behavior than the paraffin oil. Mostly lower concentration range (i.e. 0.25%w/v or below) exhibited improved antiwear behavior. On the contrary, higher concentration range (0.5%w/v or more) improved the EP properties.